Global distribution patterns of marine nitrogen-fixers by imaging and molecular methods

Running title: Diazotrophs in *Tara* Oceans

Juan José Pierella Karlusich[1,2], Eric Pelletier[2,3,], Fabien Lombard[2,5,8] , Madeline Carsique[1], Etienne Dvorak[1], Sébastien Colin[4,6,10], Marc Picheral[2,5], Francisco M. Cornejo-Castillo[4], Silvia G. Acinas[7], Rainer Pepperkok[2,6], Eric Karsenti[1,2,6], Colomban de Vargas[2,4], Patrick Wincker[2,3], Chris Bowler[1,2*], Rachel A Foster[9*]

[1] Institut de Biologie de l'ENS (IBENS), Département de biologie, École normale supérieure, CNRS, INSERM, Université PSL, 75005 Paris, France

[2] CNRS Research Federation for the study of Global Ocean Systems Ecology and Evolution, FR2022/*Tara* Oceans GOSEE, 3 rue Michel-Ange, 75016 Paris, France

[3] Génomique Métabolique, Genoscope, Institut François Jacob, CEA, CNRS, Univ Evry, Université Paris-Saclay, 91057 Evry, France

[4] Sorbonne Université, CNRS, Station Biologique de Roscoff, UMR 7144, ECOMAP, 29680 Roscoff, France

[5] Sorbonne Universités, CNRS, Laboratoire d'Océanographie de Villefranche (LOV), 06230 Villefranche-sur-Mer, France

[6] European Molecular Biology Laboratory, Heidelberg, Germany

[7] Department of Marine Biology and Oceanography, Institut de Ciènces del Mar, CSIC, Barcelona, Spain

[8] Institut Universitaire de France (IUF), Paris, France

[9] Department of Ecology, Environment and Plant Sciences, Stockholm University Stockholm Sweden

[10] Max Planck Institute for Developmental Biology, Tübingen, Germany

*corresponding authors: Rachel A Foster (rachel.foster@su.se) and Chris Bowler (cbowler@bio.ens.psl.eu)

keywords: *Tara* Oceans, diazotroph, symbioses, diatom diazotroph associations, *Richelia*, *Trichodesmium*, non-cyanobacterial diazotrophs, spheroid bodies, ultrasmall bacteria

Abstract

Biological nitrogen fixation plays a critical role in marine primary production, yet, our understanding of marine N_2-fixers (diazotrophs) is hindered by limited observations. Here, we developed a quantitative image analysis pipeline in concert with mapping of molecular markers for mining >2,000,000 images and >1,300 metagenomes in surface, deep chlorophyll maximum and mesopelagic samples across 6 size fractions (<0.2-2000 µm). Imaging and PCR-free molecular data were remarkably congruent. Sequences from diazotrophs were detected from the ultrasmall bacterioplankton (<0.2 µm) to mesoplankton (180-2000 µm), while images predicted symbiotic and colonial-forming diazotrophs (>20 µm). Imaging and molecular data estimated that polyploidy can significantly impact gene abundances of symbiotic vs colonial-forming diazotrophs. In general our results support the canonical view that larger sized diazotrophs (>10 µm) dominate the tropical belts, while sequences from unicellular cyanobacterial and non-cyanobacterial diazotrophs were globally distributed in surface and the mesopelagic. Co-occurring diazotrophic lineages of different lifestyles were frequently encountered, and several new high density regions of diazotrophs were identified in the global ocean. Overall, this work provides an update of marine diazotroph biogeographical diversity and contributes a new bio-imaging-informatic workflow.

Introduction

Approximately half of global primary production occurs in the oceans [1], fueling marine food webs, plankton decomposition and sequestration of fixed carbon to the ocean interior. Marine primary production is often limited by nitrogen (N) in vast expanses of the open ocean (approximately 75% of surface ocean) [2,3]. In these regions, the biological reduction of di-nitrogen gas (N_2) to bioavailable N, a process called biological N_2 fixation (BNF), is a critical source of new N to the ecosystem and ultimately controls the uptake and sequestration of carbon dioxide (CO_2) on geologic time scales [4–6].

In the upper sunlit ocean, it was traditionally thought that BNF was largely restricted to the subtropical and tropical gyres and mediated by a few groups of larger sized N_2-fixing (diazotrophic) cyanobacteria and holobionts (> 10 µm): the colony-forming non-heterocystous *Trichodesmium* spp., and heterocystous cyanobacterial (*Richelia intracellularis* and *Calothrix rhizosoleniae*, hereafter *Richelia* and *Calothrix,* respectively) symbionts of diatoms (diatom diazotroph associations; DDAs) [7]. More recently, unicellular cyanobacteria (UCYN) have been detected in environmental samples outside the tropical belts by qPCR targeting the BNF marker gene *nifH* [8]. One of these N_2-fixing UCYN groups is *Candidatus* Atelocyanobacterium thalassa (hereafter UCYN-A). Three UCYN-A lineages (A-1, A-2, A-3) live in symbiosis with a small single celled eukaryote (haptophyte) [9–11]. UCYN-B is another unicellular group that is most closely related to *Crocosphaera watsonii* (hereafter *Crocosphaera*). UCYN-B lives singly, colonially or in symbioses with a large chain-forming diatom

(*Climacodium frauenfeldianum)* [12–14]. UCYN-C is the third marine unicellular group identified thus far by *nifH* sequence, and is most closely related to the free-living unicellular diazotroph *Cyanothece sp.* ATCC 51142 [15], and less studied. Finally, non cyanobacterial diazotrophs (NCDs), including Archaeal and Bacterial lineages, co-occur with the cyanobacterial diazotrophs in the surface ocean and additionally below the photic layer. The distribution and *in situ* activity of NCDs are poorly constrained and difficult to estimate [16–18].

The first global ocean database of diazotrophs was compiled for the MARine Ecosystem DATa (MAREDAT) project [19]. It includes cell counts for diazotrophs that can be identified by microscopy (*Trichodesmium*, *Richelia* and *Calothrix*), as well as *nifH* qPCR datasets which additionally cover UCYN-A, UCYN-B and UCYN-C (Supplementary Fig. S1a). A recent update of the MAREDAT dataset resulted in more than doubling of the *nifH* observations [20]. However, both MAREDAT and the updated version still have low coverage in vast regions of the global ocean (Supplementary Fig. S1a). Several of these poorly sampled areas were sampled during the *Tara* Oceans circumnavigation (2009-2013) [21] (Supplementary Fig. S1b).

Tara Oceans collected discrete size fractions of plankton using a serial filtration system [21]; some samples were used to generate parallel molecular and imaging datasets. The *Tara* Oceans gene catalog from samples enriched in free-living prokaryotes is based on the assembly of metagenomes and is highly comprehensive [22,23]. However, the larger plankton size fractions (>0.8 µm) enriched in eukaryotes are genomically much more complex, and thus current *Tara* Oceans gene catalogs from

these fractions are based only on poly-A-tailed eukaryotic RNA [24,25]. Hence, the prokaryotes from these larger size fractions have been unstudied and are limited to specific taxa based on these poly-A assembled sequences [26–28], whose signal is difficult to interpret quantitatively [29]. The *Tara* Oceans imaging dataset [30] is also underutilized, especially due to the lack of well-established workflows. Overall, the cyanobacterial diazotrophs, especially those with diverse lifestyles (colonial, symbiotic, chain formers), have been poorly characterized (with the exception of UCYN-A [11,16,22,26,28,31]).

Here, we identify the diversity, abundance and distribution of symbiotic, colony-forming, and particle-associated diazotrophs in the World's ocean by mining >1,300 *Tara* Oceans metagenomes [22,24,25]. We used the single-copy core bacterial gene *recA* [32] to quantify the bacterial community in each metagenome; thus the read abundance ratio of *nifH*/*recA* provides an estimate for the relative contribution of diazotrophs. In parallel, we trained an image classification model and utilized it with images from an Underwater Vision Profiler (UVP) [33] and confocal microscopy [30] to generate a versatile analytical pipeline from images to genomics and genomics to images. Combined, our results provide an improved global overview of diazotroph abundances, diversity, and distribution (vertical and horizontal), as well as the environmental factors that shape these patterns.

Results and Discussion

Diazotroph abundance and biovolume based on imaging methods

We first used machine learning tools (see Methods [30]) to search for diazotrophs in the *Tara* Oceans high-throughput confocal imaging dataset derived from 61 samples of the 20-180 µm plankton size fraction collected at 48 different sampling locations (Supplementary Fig. S2). More than 400 images of DDAs and almost 600 images of *Trichodesmium* free filaments were predicted (Figs. 1 and 2; https://www.ebi.ac.uk/biostudies/studies/S-BSST529); all images were from the tropical and subtropical regions and consistent with the molecular analyses (see later). The same image recognition searches were performed on the confocal microscopy images from the 5-20 µm size fraction [30], which covers 75 samples from 51 stations. These searches detected only 8 images of short *Trichodesmium* filaments and 4 single *Hemiaulus-Richelia* symbiotic cells. Thus our observations are in agreement with earlier studies showing that most filaments are collected by their length rather than their diameter during sampling [34].

Several new locations not previously reported in diazotroph databases were identified (see below; Fig. 3, Supplementary Figs. S3 and S4). In addition, we detected colonies of *Crocosphaera*-like cells and others living in the more rarely reported diatom *Climacodium* [12–14]. Notably, a few *Crocosphaera* cells (1-2 cells) were detected by their strong phycoerythrin signal emitted in the alexa 546 channel while both the *Crocosphaera* cells and chloroplast of each *Climacodium* host emitted auto-fluorescence signals in the red channel (638 nm), demonstrating the

combination of signals is a key attribute in detection of inconspicuous plankton by the image recognition model (Fig. 1).

Ranges in abundances based on image analyses for the 3 main DDAs, *Hemiaulus-Richelia*, *Rhizosolenia-Richelia*, and *Chaetoceros-Calothrix,* were low and are representative of background densities (e.g., 1.5-20 symbiotic cells L^{-1}) (Fig. 3 and Supplementary Fig. S3a). The low densities and detection, especially C*haetoceros-Calothrix* which can form long chains (> 50 cells $chain^{-1}$) and the larger *Rhizosolenia-Richelia* symbioses, were not surprising given the 180 µm sieve used in the sample processing. Although *Hemiaulus-Richelia* was the most frequently detected, its chains were often short (1-2 cells), and sometimes cell integrity was compromised (i.e., broken frustules; poor auto-fluorescence). Variation in the number and length of the symbiont filaments (trichomes) was also observed and was dependent on which host the *Richelia/Calothrix* was associated (Fig. 2), consistent with previous observations [13]. Free *Richelia* and *Calothrix* filaments were also found (Supplementary Fig. S5), which are less often reported in the literature [35], but are not unexpected for facultative symbionts [36,37].

DDAs and free *Richelia*/*Calothrix* filaments were broadly distributed and detected in several new locations [19,20], including the Indian Ocean (IO), western South Atlantic Ocean (SAO), the South Pacific gyre, and the Pacific side of the Panama Canal (Supplementary Fig. S3 and S5). DDAs were concentrated in the surface, with the exception of two deeper samples of *Hemiaulus-Richelia* densities as high as in the surface: 108 m at the Hawaiin Ocean Time Series station ALOHA (A Long-Term

Oligotrophic Habitat Assessment; TARA_131; North Pacific Subtropical Gyre) and 38 m at TARA_143 (Gulf Stream, North Atlantic) (Fig. 3b). Seasonal blooms of DDAs are well known at station ALOHA, with observations of DDAs in moored sediment traps below the photic zone [38–40]. However, observations of symbiotic diatoms in the Gulf Stream are more rare [41].

We observed densities of 1-40 *Trichodesmium* free filaments L^{-1}. Similar to the DDAs, long free filaments of *Trichodesmium* were likely undersampled due to the collection and processing (35% of them are >180 µm in length). Free filaments of *Trichodesmium* co-occurred with DDAs in most stations from the IO and North Pacific Ocean (NPO) (Fig. 3a and Supplementary Fig. S4), and they were also observed at sites where DDAs were not detected, such as in the Pacific North Equatorial Current (TARA_136). Tens to hundreds of *Trichodesmium* filaments often aggregate into fusiform-shaped colonies usually referred to as 'tufts' or 'rafts' or round-shaped colonies called 'puffs' (from 200 µm to 5 mm) (Fig. 1). These dimensions were detectable and quantifiable by *in situ* imaging using the UVP5 [33] (Fig. 3 and Supplementary Fig. S4a). A total of 220 images were clearly curated as tuft or puff colonies, with the major axis ranging from 1 to 10 mm and the minor axis from 0.4 to 4 mm (https://www.ebi.ac.uk/biostudies/studies/S-BSST529). Our stringent annotation probably underestimated *Trichodesmium* colony abundances (see below the correlation with metagenomes). Colony densities were more prevalent in the NAO and NPO, while free filament densities were more abundant in the IO (Fig. 3a and Supplementary Fig. S4a), probably related to the enhanced

colony formation of *Trichodesmium* under nutrient limitation (Supplementary Fig. S6), confirming the tendencies observed in culture experiments [42].

Single-cell free-living NCDs were estimated by combining flow cytometry estimates of free-living bacterial densities with diazotroph relative abundances derived from metagenomic sequencing of the 0.22-1.6/3 µm plankton size fractions (see Methods). We detected concentrations up to ~2.8x10^6 cells L^{-1}, with the highest values in the Pacific Ocean (Fig. 3a). Our estimates agree with recent reports based on the reconstruction of metagenome-assembled genomes [16].

Combining the imaging datasets from *Tara* Oceans (flow cytometry, confocal microscopy and UVP5) enabled the conversion of abundances to estimates of biovolumes for the NCDs, *Trichodesmium* and DDAs (Fig. 3c). Single-cell free-living NCDs are by far the most abundant diazotrophs in the surface ocean, however *Trichodesmium* dominates in terms of biovolume by two orders of magnitude over NCDs (Fig. 3c). Cell density and biovolume of NCDs has not been previously reported at a global scale, thus the work presented here expands our understanding on the relative contributions for these recently recognized important diazotrophs.

Diazotroph diversity and abundance using metagenomes from size fractionated plankton samples

To gain further insights into the abundance and distribution of diazotrophs across the whole plankton size spectrum, we compared the imaging data with metagenomic reads from the 5 main size fractions mapped against a comprehensive catalog of 29,609 unique *nifH* sequences (see Methods). The *nifH* catalog represents most of

the genetic diversity reported for diazotroph isolates and environmental clone libraries (although it has some redundancy; see Methods), with 30% of the sequences derived from marine environments and the rest from terrestrial and freshwater habitats. Around 2.5% of these *nifH* sequences (762 out of 29,609) mapped with at least 80% similarity to the 1,164 metagenomes, retrieving a total of 96,215 mapped reads. Of the 762 sequences, 167 retrieved only one read. Mapped *nifH* reads were detected in slightly more than half of the samples (66% or 771 of 1,164 metagenomes), which highlights the broad distribution of diazotrophs in the *Tara* Oceans datasets (blue circles in Fig. 4a for surface waters; Supplementary Table S1).

The read abundance ratio of *nifH/recA* was used to estimate the relative contribution of diazotrophs (see Methods). Our analysis shows both a dramatic increase (up to 4 orders of magnitude) in diazotroph abundance and a compositional shift towards the larger size classes of plankton (Fig. 5). For example, diazotrophs comprise only a small proportion of the bacterial community in the 0.22-1.6/3 µm size fraction (0.004-0.8%), however, they increase to 0.003-40% in the 180-2000 µm size range (Fig. 5a). The increase is coincident with a change in taxonomy (Fig. 5b-c, Supplementary Table S1): proteobacteria and planctomycetes are the main components in the 0.22-1.6/3 µm size fraction (0.004-0.08% and 0.005-0.4%, respectively), while cyanobacterial diazotrophs dominate in the larger size fractions, including both filamentous (*Trichodesmium* and others) and non-filamentous types (free-living and symbiotic) (0.2-45% and 0.2-2%, respectively). A remarkable congruence was observed between the quantification based on imaging and metagenomic methods for the larger cyanobacterial diazotrophs (Fig. 6,

Supplementary Figs. S3ab and S4ab). Hence, a fully reversible pipeline from images to genomics and genomics to images that allows each to inform the other was developed. Hence, the image analysis enables one to quickly identify which parallel metagenomic (or metatranscriptomic) sample(s) should contain a particular diazotroph. For populations like the cyanobacterial diazotrophs which are comparatively less abundant, this approach will reduce search time in genetic analyses.

The majority (95%) of the total recruited reads mapping to the *nifH* database corresponded to 20 taxonomic groups: 5 cyanobacteria, 2 planctomycetes, and 13 proteobacteria. For the NCDs, the 2 planctomycetes and 7 of the 13 proteobacterial types corresponded to recent metagenome-assembled genomes (named HBD01 to HBD09 [16]) which additionally were among the top contributors to the *nifH* transcript pool in the 0.22-1.6/3 µm size fraction of *Tara* Oceans metatranscriptomes [22]. We also found these taxa in the larger size fractions (Figs. 5c and 7). The 0.8 µm pore-size filter enriches for larger bacterial cells, while letting pass smaller diameter cells (including the more abundant taxa: SAR11 and *Prochlorococcus*). However, it is interesting that NCDs were detected in the three largest size fractions (5-20, 20-180 or 180-2000 µm), suggesting NCDs attach to particles (e.g., marine snow, fecal pellets)[43] and/or larger eukaryotic cells/organisms, aggregate into colonies [44], or are possibly grazed by protists [45].

The main cyanobacterial taxa corresponded to *Trichodesmium*, *Richelia/Calothrix*, and UCYNs (UCYN-A1, UCYN-A2 and *Crocosphaera*). *Trichodesmium* represented

the highest number of reads for *nifH* among all diazotrophs and constituted up to 40% of the bacterial community in the three largest size fractions (Figs. 5c and 7). *Richelia nifH* reads were also detected mainly in 5-20 µm, 20-180 and 180-2000 µm, while *Calothrix* was limited to 20-180 µm. Both observations are consistent with the expected association of *Richelia*/*Calothrix* with large and small diatoms (*Hemiaulus*, *Rhizosolenia*, *Chaetoceros*) (Figs. 1, 2, 5c and 7), and the occasional report of free filaments. Free filaments were also detected in the confocal analyses (Supplementary Fig. S5; https://www.ebi.ac.uk/biostudies/studies/S-BSST529). Relative abundance of UCYN-A1 was highest in the smaller size fractions 0.2-1.6/3 µm and 0.8-5 µm, in accordance with the expected host cell size (1-3 µm) [11,46,47]. However, UCYN-A1 was also detected in the larger size fractions (5-20, 20-180 and 180-2000 µm) (Figs. 5c and 7) and suggests UCYN-A was grazed [45] and/or associated with larger particles (e.g., marine snow or aggregates [48]), which may subsequently sink to the deep ocean (see next section). *Crocosphaera* was also found in multiple size fractions (0.8-5 µm, 5-20 µm, 20-180 µm, and 180-2000 µm), which was expected given its diverse lifestyles: free-living, colonial, and symbiotic with large *Climacodium* diatoms (Fig. 1) [12–14].

Unexpectedly, *nifH* sequences with high similarity to 'spheroid bodies' (Supplementary Fig. S7a) of a few freshwater rhopalodiacean diatoms [49–51], were recruited in the surface waters of the 20-180 µm size fraction (Figs. 5c and 7). These observations were noted in multiple ocean basins (IO, SPO and SAO; Supplementary Fig. S7b). Genome analysis of 'spheroid bodies' indicates the loss of photosynthesis[52] and other metabolic pathways common to free-living cyanobacteria,

and hence they are deemed obligate to their respective hosts. Therefore, we would not expect them in the smaller size fractions. To our knowledge, this is the first genetic evidence for the presence of these populations in marine waters. Detection levels were however low (~0.5% of the total bacterioplankton community) (Figs. 5c and 7), and consistent with the expected diatom host cell diameters (approximately 30-40 µm [53]). Using published images of symbiotic rhopalodiacean diatoms [54], we manually selected similar images in the samples of interest and used them as a training set. The image recognition model predicted several images of pennate diatoms containing round granules without chlorophyll auto-fluorescence (Supplementary Fig. S7c). However our predictions are preliminary, and require further validation by other methods that are outside the scope of this work to verify whether they are indeed diazotrophic symbionts.

Evidence of polyploidy

To date, polyploidy has been reported in NCDs of soil [55,56], in some heterocystous and UCYN cyanobacteria [56–59], and in field and cultured studies of *Trichodesmium* [60]. It however remains unknown in marine NCDs, diazotrophic UCYNs and *Richelia/Calothrix* populations. Hence we cannot discount that the *nifH* abundances for the diazotrophs was not influenced by ploidy. Here we have attempted to estimate whether ploidy influences *Trichodesmium* and *Richelia*/*Calothrix* abundances since we have quantifications for both based on imaging and genetic methods from the same samples (Fig. 6). However, it is important to note that the metagenomic sampling from *Tara* Oceans was not specifically designed to quantify

metagenomic signals per seawater volume due to the lack of 'spike-ins' or DNA internal standards, and thus we have made assumptions in order to approximate estimates using the reported sampled seawater volumes and the quantity of extracted DNA (see Methods). Based on these assumptions, our results show the polyploidy for *Trichodesmium* is 410 (geometric mean of 15 points) and 177 for *Richelia*/*Calothrix* (geometric mean of 21 points), but both taxa show 5 orders of magnitude in the variability of polyploidy values according to the sample. These results expand two orders of magnitude the range of polyploidy reported previously for field and cultured populations of *Trichodesmium* (range of 1-600; [60]). Our results can be biased due to the limitations of our approach, including the lack of DNA internal standards and the low sensitivity of our methods (i. e., the use of metagenomes and high-throughput imaging dilutes the signal of specific taxa). When comparing the polyploidy of *Trichodesmium* vs *Richelia*/*Calothrix* in the 12 samples in which both are detected, the estimate for *Trichodesmium* is on average 4 times the estimate for *Richelia*/*Calothrix* (range 0.1-15). Therefore, *Trichodesmium* dominance over *Richelia*/*Calothrix* is overestimated in the metagenomes due to the higher polyploidy levels of the former. Equivalent values for NCDs and UCYNs will be needed to evaluate the effect of polyploidy in the whole diazotroph community. In addition, it is important to note that the degree of ploidy depends on the growth conditions, nutrient status, developmental stage and cell cycle [55–60].

Insights into environmental distribution and depth partitioning of diazotrophs

Diazotroph abundance was latitudinally influenced; showing expected higher relative abundances in tropical and subtropical regions, and a decrease at the equator where upwelling and higher dissolved nutrients are expected (Fig. 4). This pattern is congruent with decades of field observations (e.g., NAO, NPO) as well as modeling efforts [20,61,62], and the correlation analyses of environmental and physico-chemical variables measured during *Tara* Oceans (Fig. 8). Temperature and nutrient availability are common factors which govern diazotroph abundances [8,20,63]. Iron is also expected to be important due to the high iron requirement of the nitrogenase enzyme [64,65], therefore it was unexpected to find a less robust relationship between diazotroph abundances and modeled dissolved iron concentrations (Fig. 8a). However we cannot discount inaccuracies of modeled values relative to *in situ* bioavailable Fe concentrations.

We further analysed abundance and distribution patterns in the deeper depth samples (0-200 m and 200-1000 m, respectively). The higher numbers of N_2-fixing cyanobacteria detected in the surface (5 m) compared to the deep chlorophyll maximum (DCM; 17-188 m) in both the metagenomic and imaging datasets confirms expected distributions (Figs. 3b and 8c, also compare Fig. 9 and Supplementary Fig. S8). However, detection of both *Trichodesmium* and the DDA symbionts were nonetheless significant in some DCM samples from diverse regions: IO, SPO, and Red Sea (RS) (Supplementary Fig. S8). DDAs are expected at depth given the reported rapid sinking rates, and observations in moored sediment traps (station

ALOHA: [39,40,66]). Traditionally *Trichodesmium* has been considered to have a poor export capacity [67], however, recently there are contrary reports, and therefore *Trichodesmium* is also expected at depth [40,68,69]. Increased abundances of C*rocosphaera* co-occurred in the DCM of IO samples in the larger (5-20 µm) size fraction; indicative of the colonial and/or symbiotic lifestyles previously reported for *Crocosphaera* (Fig. 1; [12,70]). Unlike the phototrophic diazotrophs, the distribution of NCDs had no apparent depth partitioning in the epipelagic layer (Fig. 8c).

A relatively high number of *nifH* reads was detected in mesopelagic samples (128 out of 158 - or 81% - of mesopelagic samples, Supplementary Fig. S9). Although BNF and *nifH* expression has been previously reported at depth, most measurements have been made in oxygen minimum zones (OMZs; where low-oxygen waters are found) and oxygen-deficient zones (ODZs; where oxygen concentrations are low enough to induce anaerobic metabolisms) [17,22]. Here, *nifH* sequences mapped from many mesopelagic samples outside of OMZs and ODZs including in SPO, NPO, NAO and SAO (Supplementary Fig. S9). The majority of *nifH* sequences correspond to proteobacteria, however, diazotrophic cyanobacteria were also detected (Supplementary Fig. S9). In particular, 44% of total *nifH* reads in mesopelagic samples at TARA_78 and 6% at TARA_76 (of 0.2-3 µm size fraction) in SAO corresponded exclusively to UCYN-A (Supplementary Fig. S9, Supplementary Table S1). The maximum numbers of UCYN-A reads in all *Tara* Oceans samples were detected in the corresponding surface samples at these stations (Fig. 9; see below), suggesting a surface bloom. Most reports indicate the presence and activity of UCYN-A in the sunlit zone, with the exception of a study reporting UCYN-A *nifH*

sequences in shallow water sediments of the north east Atlantic ocean (seafloor 38-76 m depth) [71]. Our observation of UCYN-A at 800 m depth in the open ocean suggests that this symbiosis could contribute to carbon export despite its small cell diameter, or that other physical processes (e.g., subduction, downwelling, upwelling) in this ocean region were influencing the high detection of UCYN-A.

Global ocean biogeography of diazotrophs

Several regions displayed high densities or “hotspots” of diazotrophs which have not been previously sampled (Figs. 4 and 9, Supplementary Fig. S10). For example, in the Mozambique Channel between Madagascar and the African continent, diazotrophs constituted up to 30-40% of the bacterioplankton in the larger size fraction samples (TARA_50 to TARA_62; Figs. 4 and 9). The latter molecular results were confirmed by images of both *Trichodesmium* and symbiotic diazotrophs (Fig. 3a). Another example is the SAO near South America (TARA_76, TARA_78 and TARA_80), where UCYN-A reached 3-4% of the bacterioplankton population in the 0.8-5 µm size fraction (Figs. 4 and 9). These zones from IO and SAO represent previously undersampled regions for diazotrophs (Supplementary Fig. S1), which also lacks quantitative rate measurements for BNF [19].

The highest abundance of free-living single-cell NCDs (0.2-3 µm) corresponded to ~0.5% of the bacterioplankton in the wake of the Marquesas archipelago in the equatorial PO (TARA_123; Fig. 9). This station was reported recently as a surface planktonic bloom triggered by natural iron fertilization[72]. Other high density areas

corresponded to a few stations in the SPO (surface samples of TARA_98 and TARA_99 and DCM of TARA_102), where high abundances of proteobacteria and planctomycetes (4-33% and 8-9%, respectively) were found in larger size fractions (Fig. 9 and Supplementary Fig. S8), which likely results from association of NCDs to sinking particles. Moreover, TARA_102 is located in the Peruvian upwelling area, a region previously reported for NCDs and/or BNF activity associated with the OMZ [73–75]. These results are congruent with recent reports from the subtropical Pacific of highly diverse NCDs, some associated with sinking particles [18,75–77]. We can therefore expand the distribution of potentially particle-associated NCDs to several other ocean basins (NAO, AO, IO). Our findings emphasize the dominance and persistence of NCDs in larger size fractions of both surface and DCM, which is novel and warrants further investigation.

Many regions contain a low abundance of diazotrophs. For example, the percentages of diazotrophs in the AO, the Southern Ocean (SO), and the Mediterranean Sea (MS) reached maximum values of only 0.4, 1, and 4%, respectively (Figs. 4c and 9). The highest diazotroph abundance in the AO corresponded to NCDs found in shallow waters (20-25 m depth) of the East Siberian Sea (TARA_191; Fig. 4c and 9), a biologically undersampled region. Combined, the results concerning distribution reported here emphasize the patchy biogeographical patterns of diazotrophs.

Cyanobacterial diazotrophs are mainly found as assemblies of abundant groups

With the exception of a few stations in IO, RS, NPO and NAO where *Trichodesmium* was the main component of the mapped reads (Figs. 8b and 9, Supplementary Fig. S11), there was a general and consistent trend of co-occurrence for several cyanobacterial diazotrophs in multiple oceanic regions (Fig. 9 and Supplementary Fig. S11). For example, in the Red Sea (RS), southern IO, and at station ALOHA, both larger (*Trichodesmium*, *Richelia*) and smaller (UCYN-A, *Crocosphaera*) diameter diazotrophs were detected (Fig. 9 and Supplementary Fig. S11). In fact UCYN-A has yet to be reported in the RS, while all other cyanobacterial diazotrophs have been reported previously, including surface blooms of *Trichodesmium* spp. [78–81]. On the contrary, only small diameter diazotrophs co-dominated in the SAO; for example, UCYN-A1 and UCYN-A2 were very abundant at stations TARA_76, TARA_78 and TARA_80 (Fig. 9 and Supplementary Fig. S11). The numerous and consistent observations of mixed diazotrophic assemblages of different sizes and lifestyles (colonial, free-living, symbiotic, particle associated) highlights the need to consider how these traits enable co-occurrence.

Ultrasmall diazotrophs consist of proteobacteria and are abundant in the Arctic Ocean

Ultrasmall prokaryotes are unusual due to their reduced cell volume (these cells can pass through 0.22-μm filters, a size usually expected to exclude most microorganisms), and thus they are thought to have reduced genomes and to lack the proteins needed to carry out more complex metabolic processes. However, there is recent evidence that they do indeed participate in complex metabolisms [82]. To examine whether they may also contribute to marine BNF, we carried out the

analysis of 127 metagenomes of <0.22 µm size fractionated samples from different water layers.

A total of 79 *nifH* sequences in our database mapped with at least 80% similarity to these metagenomes, retrieving a total of 43,161 mapped reads, with the majority of the reads having high identity to proteobacterial *nifH* sequences. Of the 79 sequences, 15 retrieved only one read. Mapped *nifH* reads were detected in 92 of the 127 samples (72%), which highlights an unexpected broad distribution of ultrasmall diazotrophs (blue circles in Fig. 10a; Supplementary Table S1). Notably, when *nifH* reads were normalized by *recA* reads, we found that diazotrophs comprise up to 10% of the ultrasmall bacterioplankton, with the highest abundances detected in the AO, and in different water layers (Fig. 10a-b). This is remarkable considering that the lowest diazotroph abundance in the other size fractions was detected in the AO (Figs. 4c and 9, Supplementary Figs. S8 and S9).

The majority (84%) of the total recruited reads mapping to the *nifH* database corresponded to two sequences assembled from the <0.22 µm size-fractionated metagenomes: OM-RGC.v2.008173703 and OM-RGC.v2.008955342. The former has 99% identity to *nifH* from the epsilon-proteobacterium *Arcobacter nitrofigilis* DSM7299 [83] (hereafter *Acrobacter*), the second is more close in sequence identity to gamma-proteobacteria. The *Acrobacter*-like sequence only retrieved reads from surface and DCM, while the gamma-proteobacterium-like retrieved reads from surface, DCM and mesopelagic (Fig. 10c). Both sequences also retrieved reads from other sizes fractions (Fig. 7 and Supplementary Fig. S12). Members of *Arcobacter* genus are either symbionts or pathogens [83], which is inconsistent with >9% of ultrasmall bacterioplankton associated with the <0.22 µm size fraction in the DCM

waters of station TARA_158 (Supplementary Fig. S12). An additional proteobacterial sequence (OM-RGC.v2.008817394) exclusively retrieved reads from the <0.22 µm size fractionated samples (Supplementary Fig. S12). Combined, these results prompt the inclusion of ultrasmall diazotrophs in future field surveys to quantify their potential ecological and biogeochemical importance.

Conclusions

This is the first attempt to assess the diversity, abundance, and distribution of diazotrophs at a global ocean scale using paired image and PCR-free molecular analyses. Unlike earlier studies, our work included the full biological and ecological complexity of diazotrophs: i.e., unicellular, colonial, particle associated, symbiotic, cyanobacteria and NCDs. Our work also enabled estimates of total diazotrophic biovolume in several layers of the global ocean. Diazotrophs were found to be globally distributed and present in all size fractions, even among ultrasmall bacterioplankton (<0.22 µm), which were especially abundant in the AO. Unexpectedly, we detected sequences similar to obligate symbionts of freshwater diatoms nearly exclusively in the larger size fraction (20-180 µm) and in multiple and geographically distinct samples (IO, SPO, SAO). We did not find strong evidence for widespread distributions for UCYNs, which was unexpected given the results from a decade of past observations (although we cannot discount the influence of seasonal sampling biases). On the contrary, the highest abundance of UCYN-A was restricted to an area of the SAO where we found UCYN-A at depth and in surface samples, suggesting a potential mechanism for carbon export in spite of the small expected

size of these symbiotic cells, or the effect of other physical processes (e.g., subduction, downwelling, upwelling). A major conclusion from our work is the identification of new hotspots for diazotrophs in previously undersampled regions of the global ocean, for example, in several locations of the IO.

Both the morphological and molecular data support the canonical view of *Trichodesmium* dominance, rather than more recent suggestions that have emphasized the importance of UCYNs. Historically and recently, the field has attempted to make paradigm shifts in favor of one dominant group (large vs. small diameter cyanobacterial diazotrophs). The data presented here on the contrary argues in favor of regions of co-existing assemblages of cyanobacterial diazotrophs with diverse lifestyles (colonial, free-living, symbiotic, particle associated), while NCDs appear ubiquitously distributed. Overall, this work provides an updated composite of diazotroph biogeography in the global ocean, providing valuable information in the context of global change and the substantial anthropogenic perturbations to the marine nitrogen cycle.

Methods

Tara Oceans sampling

Tara Oceans performed a worldwide sampling of plankton between 2009 and 2013 (Supplementary Fig. S1b). Three different water depths were sampled: surface (5 m depth), DCM (17–188 m), and mesopelagic (200–1000 m) (Supplementary Fig. S2). The plankton were separated into discrete size fractions using a serial filtration system [21]. Given the inverse logarithmic relationship between plankton size and

abundance [21,84], higher seawater volumes were filtered for the larger size fractions (10-10^5 L; see Table 1 and Fig. 5 in [21]). Taking into account that diazotrophs are less abundant than sympatric populations and have a wide size variation (Fig. 1), a comprehensive perspective requires analyses over a broad spectrum, which to date has been lacking. Five major organismal size fractions were collected: picoplankton (0.2 to 1.6 µm or 0.2 to 3 µm; named here 0.2-1.6/3 µm size fraction), piconanoplankton (0.8 to 5 µm or 0.8 to 2000 µm; named here 0.8-5 µm size fraction), nanoplankton (5 to 20 µm or 3 to 20 µm; named here 5-20 µm size fraction), microplankton (20 to 180 µm), and mesoplankton (180 to 2000 µm) (Supplementary Fig. S2) [21]. In addition, ultrasmall plankton (<0.22 µm) were also collected (Supplementary Fig. S2) [21]. The *Tara* Oceans datasets used in the present work are listed in Supplementary Fig. S2 and specific details about them and their analysis are described below.

Read recruitment of marker genes in metagenomes

The use of metagenomes avoids the biases linked to the PCR amplification steps of metabarcoding methods, and thus it is better for quantitative observations. This is especially important for protein-coding gene markers, such as *nifH*, which display high variability in the third position of most codons, and thus necessitate the use of highly degenerate primers for a broad taxonomic coverage [85]. The detection of low-abundance organisms, such as diazotrophs, is facilitated by the deep sequencing of the *Tara* Oceans samples (between ~10^8 and ~10^9 total metagenomic reads per sample) [22,24,25]. The 1,326 metagenomes generated by the expedition are derived from 147 globally distributed stations and three different water layers: 745

metagenomes from surface, 382 from DCM (17–188 m) and 41 from the bottom of the mixed layer when no DCM was observed (25-140 m), and 158 from mesopelagic (200–1000 m) (Supplementary Fig. S2).

The read abundance of the single-copy gene *recA* was used to estimate the total bacterial community abundance in each sample (in contrast to the widely used 16S rRNA gene, which varies between one and fifteen copies among bacterial genomes [86,87]). For simplicity, we assumed that *nifH* is also a single-copy gene, so the abundance ratio of *nifH/recA* provides an estimate for the relative contribution of diazotrophs to the total bacterial community. However, we realize that there are examples of 2-3 *nifH* copies in heterocyst-forming cyanobacteria such as *Anabaena variabilis* and *Fischerella* sp. [88,89], or in the firmicutes *Clostridium pasteurianum* [90], and that we are not taking into account the polyploidy effect.

The metagenomes were aligned against sequence catalogs of marker genes for diazotrophs (*nifH*) and bacteria (*recA*) (Supplementary Tables S2 and S3). The analysis was carried out using bwa tool version 0.7.4 [91] using the following parameters: -minReadSize 70 -identity 80 -alignment 80 -complexityPercent 75 -complexityNumber 30. The *nifH* sequence catalog (hereafter *nifH* database) was composed of 29,175 publicly available unique sequences from the laboratory of JP Zehr (University of California, Santa Cruz, USA; version April 2014; https://www.jzehrlab.com). Although the Zehr database has some redundancy (9,048 out of the 29,175 total unique sequences are retained when clustered at 95% identity using CDHIT-EST tool [92]), all non-identical sequences were used to maximize the number of metagenomic mapping reads. Moreover, this database was complemented with additional *nifH* genes retrieved from the sequenced genomes of

Integrated Microbial Genome database (IMG) [93] and from different *Tara* Oceans datasets: Ocean Microbial Reference Gene Catalog version 2 (OM-RGC-v2 [22]), assemblies [16] and 10 clones (this study). *nifH* clone libraries were built using DNA extracted from 0.2-1.6/3 µm size fraction plankton samples as described in Alberti et al [24]. DNA samples from the same oceanic region were pooled together at a concentration of 10 ng/µl and used as template in a nested *nifH* PCR using degenerate primers [94]. Five PCR products were purified and cloned using the TOPO-TA cloning kit (Invitrogen). Inserts were Sanger-sequenced bidirectionally using M13 Forward and M13 Reverse vector primers following manufacturer's recommendations. A total of 411 *nifH* clone sequences were generated, among which 148 showed less than 95% nucleotide identity with any previously published sequence. These novel sequences were grouped into clusters sharing more than 99% nucleotide identity and represented by 10 consensus sequences (Supplementary Table S2). The *recA* sequences were obtained from sequenced genomes in IMG [93] and from OM-RGC-v2 [22]. Homologous sequences were included in the two catalogs as outgroups to minimize false positive read alignments. These latter sequences were retrieved from IMG, OM-RGC-v2 and the Marine Microbial Eukaryotic Transcriptome Sequencing Project (MMETSP [95]) using HMMer v3.2.1 with gathering threshold option (http://hmmer.org/). The outgroups for *recA* consisted of sequences coding for the RecA Pfam domain (PF00154), including RADA and RADB in Archaea, RAD51 and DCM1 in eukaryotes, and UvsX in viruses [96]. Outgroups for *nifH* consisted of sequences coding for the Pfam domain Fer4_NifH (PF00142), including a subunit of the pigment biosynthesis complexes protochlorophyllide reductase and chlorophyllide reductase [97].

Phylogenetic analysis of recruited metagenomic reads

To support the taxonomic affiliation of metagenomic reads recruited by *nifH* sequences from 'spheroid bodies', we carried out a phylogenetic reconstruction in the following way. The translated metagenomic reads were aligned against a NifH reference alignment using the option --add of MAFFT version 6 with the G-INS-I strategy [98]. The resulting protein alignment was used for aligning the corresponding nucleotide sequences using TranslatorX [99] and phylogenetic trees were generated using the HKY85 substitution model in PhyML version 3.0 [100]. Four categories of rate variation were used. The starting tree was a BIONJ tree and the type of tree improvement was subtree pruning and regrafting. Branch support was calculated using the approximate likelihood ratio test (aLRT) with a Shimodaira–Hasegawa-like (SH-like) procedure.

Flow cytometry data and analysis

Picoplankton samples were prepared for flow cytometry from three aliquots of 1 ml of seawater (pre-filtered through 200-µm mesh), as described in [23,101]. For quantifying the densities of single-cell free-living diazotrophs, we combined the cell density measurements from flow cytometry with the relative abundances derived from molecular methods as done by Props et al. [102]. Specifically, we multiplied the bacterial concentration derived from flow cytometry by the *nifH* to *recA* ratio of metagenomic read abundances from samples of size fraction 0.22-1.6/3 µm. For biovolume estimations of single-cell free-living diazotrophs, we assumed an average

cell biovolume of 1 μm^3 based on the cell dimensions reported in literature for cultured NCDs [103–108].

Detection of diazotrophs in the confocal laser-scanning microscopy dataset

Quantitative microscopy was performed using environmental High Content Fluorescence Microscopy (eHCFM) [30] on i) 61 samples collected at 48 different stations using a microplankton net (20 µm mesh size) and filtering the codend volume through a 180 µm sieve; ii) 75 samples collected at 51 stations using a nano plankton net (5 µ mesh size) and filtering the coded volume through a 20 µm sieve (Supplementary Fig. S2). Sample collection and preparation as well imaging acquisition is described in [30]. Briefly, samples were fixed on board *Tara* in 10% monomeric formaldehyde (1 % final concentration) buffered at pH 7.5 and 500 µl EM grade glutaraldehyde (0.25% final concentration) and kept at 4 °C until analysis. Cells were imaged by Confocal Laser Scanning Microscopy (Leica Microsystem SP8, Leica Germany), equipped with several laser lines (405 nm, 488 nm, 552 nm, 638 nm). The 5-20 µm size fraction was imaged with the water immersion lens HC PL APO 40x/1,10 mot CORR CS2 objective, and the 20-180 µm size fraction was imaged with the HC PL APO 20x/0.75IMM CORR CS2 objective. Multiple fluorescent dyes were used to observe the cellular components of the organisms, including: the nuclei (blue, Hoechst, Ex405 nm /Em420-470 nm), cellular membranes (green, DiOC6(3), Ex488 nm /Em500-520 nm), cell surface (cyan, AlexaFluor 546, Ex552 nm /Em560-590 nm), and chlorophyll autofluorescence (red, Ex638 nm /Em680-700 nm).

We used the confocal microscopy data to quantify DDAs and free filaments of *Trichodesmium* for abundance and biovolume. Image classification and annotation was carried out using the Ecotaxa web platform [109] in the following way. We first manually searched for the target taxa and curated an initial training set in a few samples where molecular methods detected high abundances (i.e., high metagenomic read abundance of *nifH*), obtaining 53 images for DDAs and 80 for *Trichodesmium* filaments. This training set was then used for automating the classification of the whole dataset by means of supervised machine learning (random forest) based on a collection of 480 numeric 2D/3D features [30]. The predictions were, in turn, manually curated and used as a new training set, repeating this step iteratively until no new images appeared. Other taxonomic groups were also annotated and used as outgroups to improve the predictions of our taxa of interest. Abundance estimates were normalized based on the total sample volumes as cells L^{-1} (see below). DDAs are enumerated as symbiotic cells L^{-1}, while *Trichodesmium* are filaments L^{-1}. We used the major and minor axis of every image to calculate their ellipsoidal equivalent biovolume.

Ploidy calculation for *Trichodesmium* and *Richelia*/*Calothrix*

For ploidy calculations, we used the paired confocal microscopy imaging and metagenomes obtained from the same 20-180-μm size-fractionated samples, thus dividing the cells L^{-1} by the *nifH* copies L^{-1}. A known volume of seawater (Vs, L) was filtered and recorded through the plankton net (20 μm mesh). Contents of the codend were filtered through a 180 μm sieve and diluted to 3L. 45ml of the diluted cod end

was fixed with 5ml formaldehyde (1% final) and glutaraldehyde (0.25% final) [30], and kept at 4° C. A sub-sample volume (Vi, liter) was mounted into an optical multi-well plate for automated confocal imaging and adjusted to avoid the saturation of the well bottom. The well bottom area (86mm²) was fully imaged. The organisms were segmented from the images, and then identified and counted. Hence, the estimate of the abundance (A) per liter of a given biological group in the original seawater is provided by : A = #occurrence / (Vi x Cf) ; the concentration factor Cf = (Vs/ 3 L) x (45/50). The number of *Richelia*/*Calothrix* filaments per host and number cells per filament in *Trichodesmium* and *Richelia*/*Calothrix* were enumerated manually, thus obtaining the values of cells L^{-1} in each sample.

For nucleic acid isolation, 1000 mL were sampled from the diluted codend and filtered onto 47mm diameter 10µm pore size polycarbonate membrane filters (one to four membrane filters, n, depending on the sample), and immediately flash-frozen. DNA extraction was performed from one membrane as described by [24]. Of the extracted DNA ($DNA_{extracted}$, ng), a quantity was used for DNA library preparation and sequencing process using Illumina machines (Illumina, USA) [24]. Thus, we calculated the *nifH* copies L^{-1} for each taxa using the number of reads mapping the *nifH* reference sequences of the taxon of interest ($reads_{nifH\text{-}taxon}$) among the total number of sequenced reads ($reads_{total}$). We assumed 100% efficiency of DNA extraction for *Trichodesmium* and *Richelia*/*Calothrix* and a *nifH* gene length of 750 bp (which implies $1.21x10^9$ *nifH* copies / *nifH* ng). Hence, the estimate of the *nifH* copies (C) per liter of a given biological group in the original seawater is provided by $C= DNA_{extracted} * (1.21x10^9$ copies *nifH* / ng *nifH*) * $reads_{nifH\text{-}taxon}$ / $reads_{total}$ / (Vs / (3 L * n)).

Underwater Vision Profiler dataset and analysis

The Underwater Vision Profiler 5 (UVP5, Hydroptics, France) [33] is an underwater imager mounted on the Rosette Vertical Sampling System. This system illuminates precisely calibrated volumes of water and captures images during the descent (5-20 images s^{-1}). The UVP5 was operated *in situ* and was designed to detect and count objects of >100 µm in length and to identify those of >600 µm in size. In the current work, we used this method for the quantification of *Trichodesmium* colony abundance and biovolume. The search, curation and annotation of the corresponding images and their biovolume determination were carried out as described in the previous section. Only images clearly curated as tuft or puff colonies were used to avoid false positives (faecal pellets, large diatom chains, etc). However, this stringent classification underestimated these colonies given the numerous stations without *in situ* UVP5 images annotated as *Trichodesmium* colonies but with detection of *Trichodesmium nifH* in the metagenomes of the 180-2000 µm size fractionated samples (Fig. 6c). This pattern can also be produced if *Trichodesmium* colonies do not pass the filter holes of 2000 µm in diameter, but given that they are known to be fragile, it is probable that most of them pass it either undamaged or fragmented.

Determination of contextual physicochemical parameters

Measurements of temperature were recorded at the time of sampling using the vertical profile sampling system (CTD-rosette) (https://doi.org/10.1594/PANGAEA.836319 and

https://doi.org/10.1594/PANGAEA.836321). Dissolved nutrients (NO^-_3, PO_4) were analyzed according to previous methods [110,111] with detection limits of 0.05 and 0.02 µmol L^{-1}, respectively. Iron levels were derived from a global ocean biogeochemical model [112].

Plotting and statistical analysis

Graphical analyses were carried out in R language (http://www.r-project.org/) using *ggplot2* [113] and treemaps were generated with *treemap*. The trends between diazotroph abundance and latitude were displayed with generalized additive models using the *geom_smooth* function of *ggplot2* [113]. Metric multidimensional scaling (NMDS) analysis to visualize Bray-Curtis distances was carried out with the *metaMDS* command in the R package *vegan* [114], and the influence of environmental variables on sample ordination was evaluated with the function *envfit* in the same R package. Hierarchical agglomerative clustering of samples using average linkage was performed with the function *hclust* of the R package *stats*.

Data availability

Contextual data [21]: https://doi.org/10.1594/PANGAEA.875582; flow cytometry [23,101]: http://dx.doi.org/10.17632/p9r9wttjkm.2; high throughput confocal microscopy images [30] of 5-20 µm sized-fractionated samples: https://ecotaxa.obs-vlfr.fr/prj/3365; high throughput confocal microscopy images [30] of 20-180 µm sized-fractionated samples: https://ecotaxa.obs-vlfr.fr/prj/2274; UVP5 images [33]: https://ecotaxa.obs-vlfr.fr/prj/579. The confocal microscopy and UVP5 images annotated as diazotrophs in the current work and their corresponding metadata were

submitted to the EMBL-EBI repository BioStudies (www.ebi.ac.uk/biostudies) under accession S-BSST529. *Tara* Oceans metagenomes [22,24,25] are archived at ENA under the accession numbers: PRJEB1787, PRJEB1788, PRJEB4352, PRJEB4419, PRJEB9691, PRJEB9740 and PRJEB9742. The 10 novel *nifH* sequences generated in the clone libraries of the current work were submitted to ENA under the accession numbers: MW590317-MW590326.

Acknowledgements.

We would like to thank all colleagues from the *Tara* Oceans consortium as well as the *Tara* Ocean Foundation for their inspirational vision. We also acknowledge the current and past members of the laboratory of JP Zehr for the curation and public access to the *nifH* database. We are grateful with Lionel Guidi, Stéphane Pesant, and Julie Poulain for acquiring information on *Tara* Oceans sampling, Luca Santangeli from EMBL Heidelberg for confocal microscopy image acquisition and Luis Pedro Coelho (currently at Fudan University) for image processing, Benjamin Blanc from Laboratoire d'Océanographie de Villefranche-sur-mer for help with UVP5 image processing and annotation, Daniel Lundin from Linnaeus University for his analytical support and advice, Tom Delmont from Genoscope for his useful discussions, Flora Vincent from Weizmann Institute of Science for her help with Ecotaxa resource, Eric Bapteste, Philippe Lopez and Romain Lannes from Sorbonne Université for their advice with ultrasmall bacteria analysis. This work has been supported by the FFEM - French Facility for Global Environment, French Government 'Investissements d'Avenir' programmes OCEANOMICS (ANR-11-BTBR-0008), FRANCE GENOMIQUE (ANR-10-INBS-09-08), MEMO LIFE

(ANR-10-LABX-54), and PSL Research University (ANR-11-IDEX-0001-02). R.A.F. acknowledges funding from Knut and Alice Wallenberg foundation. C.B. acknowledges funding from the European Research Council (ERC) under the European Union's Horizon 2020 research and innovation programme (Diatomic; grant agreement No. 835067) and Agence Nationale de la Recherche "Phytomet" (ANR-16-CE01-0008) projects. F.M.C-C. acknowledges funding from the European Union's Horizon 2020 research programme under the Marie Sklodowska-Curie grant agreement No. 749380 (UCYN2PLAST). S.G.A acknowledges funding from the project "MAGGY" (CTM2017-87736-R) from the Spanish Ministry of Economy and Competitiveness and the 'Severo Ochoa Centre of Excellence' accreditation (CEX2019-000928-S). J.J.P.K. acknowledges postdoctoral funding from the Fonds Français pour l'Environnement Mondial. This article is contribution number ** of *Tara* Oceans.

Author contributions

RAF and CB designed the study and supervised the project. RAF, CB and JJPK wrote the paper with substantial input from all co-authors. JJPK compiled the marker gene catalogs and EP performed the metagenomic mapping. RP, SC and EK set up the imaging platform for the e-HFCM data generation and processing. JJPK, RAF, MC, ED, FL, SC performed the taxonomic annotation of the e-HFCM dataset. FMC-C and SGA generated the *nifH* clone libraries. MP performed the collection and taxonomic annotation of UVP5 dataset. JJPK performed the formal analysis and visualization.

Competing financial interests: The authors declare no competing financial interests.

References

1. Field, C. B., Behrenfeld, M. J., Randerson, J. T. & Falkowski, P. Primary production of the biosphere: integrating terrestrial and oceanic components. *Science* **281**, 237–240 (1998).
2. Moore, C. M. et al. Processes and patterns of oceanic nutrient limitation. *Nat. Geosci.* **6**, 701–710 (2013).
3. Tyrrell, T. The relative influences of nitrogen and phosphorus on oceanic primary production. *Nature* **400**, 525–531 (1999).
4. Falkowski, P. G. Evolution of the nitrogen cycle and its influence on the biological sequestration of CO_2 in the ocean. *Nature* **387**, 272–275 (1997).
5. Karl, D. et al. The role of nitrogen fixation in biogeochemical cycling in the subtropical North Pacific Ocean. *Nature* **388**, 533–538 (1997).
6. Capone, D. G. et al. Nitrogen fixation by *Trichodesmium spp*.: An important source of new nitrogen to the tropical and subtropical North Atlantic Ocean. *Global Biogeochem. Cycles* **19**, GB2024 (2005).
7. Capone, D. G. *Trichodesmium*, a globally significant marine cyanobacterium. *Science* **276**, 1221–1229 (1997).
8. Moisander, P. H. et al. Unicellular cyanobacterial distributions broaden the oceanic N_2 fixation domain. *Science* **327**, 1512–1514 (2010).
9. Thompson, A. W. et al. Unicellular cyanobacterium symbiotic with a single-celled eukaryotic alga. *Science* **337**, 1546–1550 (2012).
10. Farnelid, H., Turk-Kubo, K., Muñoz-Marín, M. C. & Zehr, J. P. New insights into the ecology of the globally significant uncultured nitrogen-fixing symbiont UCYN-A. *Aquat. Microb. Ecol.* **77**, 125–138 (2016).
11. Cornejo-Castillo, F. M. et al. UCYN-A3, a newly characterized open ocean sublineage of the symbiotic N_2 -fixing cyanobacterium *Candidatus* Atelocyanobacterium thalassa. Environ. Microbiol. **21**, 111–124 (2019).
12. Carpenter, E. J. & Janson, S. Intracellular symbionts in the marine diatom *Climacodium frauenfeldianum* Grunow (Bacillariophyceae). *J. Phycol.* **36**, 540–544 (2000).
13. Caputo, A., Nylander, J. A. A. & Foster, R. A. The genetic diversity and evolution of diatom-diazotroph associations highlights traits favoring symbiont integration. *FEMS Microbiol. Lett*. **366**, fnz120 (2019).
14. Webb, E. A., Ehrenreich, I. M., Brown, S. L., Valois, F. W. & Waterbury, J. B. Phenotypic and genotypic characterization of multiple strains of the diazotrophic cyanobacterium, *Crocosphaera watsonii*, isolated from the open ocean. *Environ. Microbiol.* **11**, 338–348 (2009).
15. Foster, R. A. et al. Influence of the Amazon River plume on distributions of free-living and symbiotic cyanobacteria in the western tropical north Atlantic Ocean. *Limnol. Oceanogr*. **52**, 517–532 (2007).
16. Delmont, T. O. et al. Nitrogen-fixing populations of Planctomycetes and Proteobacteria are abundant in surface ocean metagenomes. *Nat Microbiol* **3**, 804–813 (2018).

17. Moisander, P. H. et al. Chasing after non-cyanobacterial nitrogen fixation in marine pelagic environments. *Front. Microbiol*. **8**, 1736 (2017).
18. Farnelid, H. et al. Nitrogenase gene amplicons from global marine surface waters are dominated by genes of non-cyanobacteria. *PLoS One* **6**, e19223 (2011).
19. Luo, Y.-W. et al. Database of diazotrophs in global ocean: abundance, biomass and nitrogen fixation rates. *Earth Syst. Sci. Data* **4**, 47–73 (2012).
20. Tang, W. & Cassar, N. Data-Driven Modeling of the Distribution of Diazotrophs in the Global Ocean. *Geophys. Res. Lett*. **46**, 12258–12269 (2019).
21. Pesant, S. et al. Open science resources for the discovery and analysis of *Tara* Oceans data. *Sci Data* **2**, 150023 (2015).
22. Salazar, G. et al. Gene expression changes and community turnover differentially shape the global ocean metatranscriptome. *Cell* 179, 1068–1083.e21 (2019).
23. Sunagawa, S. et al. Structure and function of the global ocean microbiome. *Science* **348**, 1261359 (2015).
24. Alberti, A. et al. Viral to metazoan marine plankton nucleotide sequences from the *Tara* Oceans expedition. *Sci Data* **4**, 170093 (2017).
25. Carradec, Q. et al. A global ocean atlas of eukaryotic genes. *Nat. Commun*. **9**, 373 (2018).
26. Cornejo-Castillo, F. M. et al. Cyanobacterial symbionts diverged in the late Cretaceous towards lineage-specific nitrogen fixation factories in single-celled phytoplankton. *Nat. Commun*. **7**, 11071 (2016).
27. Cornejo-Castillo, F. M. & Zehr, J. P. Intriguing size distribution of the uncultured and globally widespread marine non-cyanobacterial diazotroph Gamma-A. *ISME J.* **15**, 124–128 (2020).
28. Vorobev, A. et al. Transcriptome reconstruction and functional analysis of eukaryotic marine plankton communities via high-throughput metagenomics and metatranscriptomics. *Genome Res*. **30**, 647–659 (2020).
29. Güell M, Yus E, Lluch-Senar M & Serrano L Bacterial transcriptomics: what is beyond the RNA horiz-ome? *Nat. Rev. Microbiol.* **9**, 658–69 (2011).
30. Colin, S. et al. Quantitative 3D-imaging for cell biology and ecology of environmental microbial eukaryotes. E*life* **6**, e26066 (2017).
31. Cabello, A. M. et al. Global distribution and vertical patterns of a prymnesiophyte-cyanobacteria obligate symbiosis. *ISME J*. **10**, 693–706 (2016).
32. Sunagawa, S. et al. Metagenomic species profiling using universal phylogenetic marker genes. *Nat. Methods* **10**, 1196–1199 (2013).
33. Picheral, M. et al. The Underwater Vision Profiler 5: An advanced instrument for high spatial resolution studies of particle size spectra and zooplankton. *Limnol. Oceanogr.: Methods* **8**, 462–473 (2010).
34. Tenório, M. M. B., Dupouy, C., Rodier, M., & Neveux, J. *Trichodesmium* and other planktonic cyanobacteria in New Caledonian waters (SW tropical Pacific) during an El Niño episode. *Aquat. Microb. Ecol.*, **81**, 219-241 (2018).
35. Gómez, F., Furuya, K. & Takeda, S. Distribution of the cyanobacterium *Richelia intracellularis* as an epiphyte of the diatom *Chaetoceros compressus* in the western Pacific Ocean. *J. Plankton Res*. **27**, 323–330 (2005).
36. Villareal, T. A. Laboratory culture and preliminary characterization of the nitrogen-fixing *Rhizosolenia-Richelia* symbiosis. *Mar. Ecol.* **11**, 117–132 (1990).

37. Foster, R. A., Goebel, N. L. & Zehr, J. P. Isolation of *Calothrix rhizosoleniae* (cyanobacteria) strain SC01 from *Chaetoceros* (Bacillariophyta) spp. diatoms of the Subtropical North Pacific Ocean. *J. Phycol*. **46**, 1028–1037 (2010).
38. Karl, D. M., Church, M. J., Dore, J. E., Letelier, R. M. & Mahaffey, C. Predictable and efficient carbon sequestration in the North Pacific Ocean supported by symbiotic nitrogen fixation. *Proc. Natl Acad. Sci.* **109**, 1842–1849 (2012).
39. Scharek, R., Tupas, L. M. & Karl, D. M. Diatom fluxes to the deep sea in the oligotrophic North Pacific gyre at Station ALOHA. *Mar. Ecol. Prog. Ser*. 182, 55–67 (1999).
40. Scharek, R., Latasa, M., Karl, D. M. & Bidigare, R. R. Temporal variations in diatom abundance and downward vertical flux in the oligotrophic North Pacific gyre. *Deep Sea Res. Part I Oceanogr. Res. Pap*. **46**, 1051–1075 (1999).
41. Ratten, J.-M. et al. Sources of iron and phosphate affect the distribution of diazotrophs in the North Atlantic. *Deep Sea Res. Part II Top. Stud. Oceanogr*. **116**, 332–341 (2015).
42. Tzubari, Y., Magnezi, L., Be'er, A. & Berman-Frank, I. Iron and phosphorus deprivation induce sociality in the marine bloom-forming cyanobacterium *Trichodesmium*. *ISME J*. **12**, 1682–1693 (2018).
43. Geisler, E., Bogler, A., Rahav, E. & Bar-Zeev, E. Direct detection of heterotrophic diazotrophs associated with planktonic aggregates. *Sci. Rep*. **9**, 9288 (2019).
44. Bentzon-Tilia, M., Severin, I., Hansen, L. H., & Riemann, L. Genomics and ecophysiology of heterotrophic nitrogen fixing bacteria isolated from estuarine surface water. *mBio* **6**, e929-15. (2015).
45. Scavotto, R. E., Dziallas, C., Bentzon-Tilia, M., Riemann, L. & Moisander, P. H. Nitrogen-fixing bacteria associated with copepods in coastal waters of the North Atlantic Ocean. *Environ. Microbiol.* **17**, 3754–3765 (2015).
46. Foster, R. A. & Zehr, J. P. Diversity, genomics, and distribution of phytoplankton-cyanobacterium single-cell symbiotic associations. *Annu. Rev. Microbiol*. **73**, 435–456 (2019).
47. Tripp, H. J. et al. Metabolic streamlining in an open-ocean nitrogen-fixing cyanobacterium. *Nature* **464**, 90–94 (2010).
48. Farnelid, H. et al. Diverse diazotrophs are present on sinking particles in the North Pacific Subtropical Gyre. *ISME J*. **13**, 170–182 (2019).
49. Drum, R. W. & Pankratz, S. Fine structure of an unusual cytoplasmic inclusion in the diatom genus, *Rhopalodia*. *Protoplasma* **60**, 141–149 (1965).
50. Nakayama, T. & Inagaki, Y. Genomic divergence within non-photosynthetic cyanobacterial endosymbionts in rhopalodiacean diatoms. *Sci. Rep*. **7**, 13075 (2017).
51. Prechtl, J., Kneip, C., Lockhart, P., Wenderoth, K. & Maier, U.-G. Intracellular spheroid bodies of *Rhopalodia gibba* have nitrogen-fixing apparatus of cyanobacterial origin. *Mol. Biol. Evol*. **21**, 1477–1481 (2004).
52. Nakayama, T. et al. Complete genome of a nonphotosynthetic cyanobacterium in a diatom reveals recent adaptations to an intracellular lifestyle. *Proc. Natl Acad. Sci.* **111**, 11407–11412 (2014).
53. Patrick, R. & Reimer, C. W. The diatoms of the United States: Exclusive of Alaska and Hawaii. Volume 2, Part 1, Entomoneidaceae, Cymbellaceae, Gomphonemaceae, Epithemiaceae. (1975).

54. Stancheva, R. et al. Nitrogen-fixing cyanobacteria (free-living and diatom endosymbionts): their use in southern California stream bioassessment. *Hydrobiologia* **720**, 111–127 (2013).
55. Maldonado, R., Jimenez, J. & Casadesus, J. Changes of ploidy during the *Azotobacter vinelandii* growth cycle. *J. Bacteriol*. **176**, 3911–3919 (1994).
56. Simon, R. D. Macromolecular composition of spores from the filamentous cyanobacterium *Anabaena cylindrica*. *J Bacteriol*: **129**, 1154–1155 (1977).
57. Simon, R. D. DNA content of heterocysts and spores of the filamentous cyanobacterium *Anabaena variabilis*. *FEMS Microbiol. Lett*. **8.4**: 241-245 (1980).
58. Griese, M., Lange, C. & Soppa, J. Ploidy in cyanobacteria. *FEMS Microbiol. Lett.* **323**, 124–131 (2011).
59. Sukenik, A., Kaplan-Levy, R., Welch, J. & Post, A.F. Massive multiplication of genome and ribosomes in dormant cells (akinetes) of *Aphanizomenon ovalisporum* (Cyanobacteria). *ISME J* **6**, 670–679 (2012).
60. Sargent, E. C. et al. Evidence for polyploidy in the globally important diazotroph *Trichodesmium. FEMS Microbiol. Lett.* **363**, fnw244 (2016).
61. Dutkiewicz, S., Ward, B. A., Monteiro, F. & Follows, M. J. Interconnection of nitrogen fixers and iron in the Pacific Ocean: Theory and numerical simulations. *Global Biogeochem. Cycles* **26**, GB1012 (2012).
62. Deutsch, C., Sarmiento, J. L., Sigman, D. M., Gruber, N. & Dunne, J. P. Spatial coupling of nitrogen inputs and losses in the ocean. *Nature* **445**, 163–167 (2007).
63. Mills, M. M., Ridame, C., Davey, M., La Roche, J. & Geider, R. J. Iron and phosphorus co-limit nitrogen fixation in the eastern tropical North Atlantic. *Nature* **429**, 292–294 (2004).
64. Raven, J. A. The iron and molybdenum use efficiencies of plant growth with different energy, carbon and nitrogen sources. *New Phytol*. **109**, 279–287 (1988).
65. Kustka, A. B. et al. Iron requirements for dinitrogen- and ammonium-supported growth in cultures of *Trichodesmium* (IMS 101): Comparison with nitrogen fixation rates and iron: carbon ratios of field populations. *Limnol. Oceanogr*. **48**, 1869–1884 (2003).
66. Subramaniam, A. et al. Amazon River enhances diazotrophy and carbon sequestration in the tropical North Atlantic Ocean. *Proc. Natl. Acad. Sci. U. S. A.* **105**, 10460–10465 (2008).
67. Walsby, A. E. The gas vesicles and buoyancy of *Trichodesmium*. in *Marine pelagic cyanobacteria:* Trichodesmium *and other diazotrophs*, 141–161 (Springer Netherlands, 1992).
68. Rouco, M. et al. Variable depth distribution of *Trichodesmium* clades in the North Pacific Ocean. *Environ. Microbiol. Rep.* **8**, 1058–1066 (2016).
69. Pabortsava, K. et al. Carbon sequestration in the deep Atlantic enhanced by Saharan dust. *Nat. Geosci*. **10**, 189–194 (2017).
70. Foster, R. A., Sztejrenszus, S. & Kuypers, M. M. M. Measuring carbon and N_2 fixation in field populations of colonial and free-living unicellular cyanobacteria using nanometer-scale secondary ion mass spectrometry. *J. Phycol*. **49**, 502–516 (2013).
71. Brown, S. M. & Jenkins, B. D. Profiling gene expression to distinguish the likely active diazotrophs from a sea of genetic potential in marine sediments. *Environ Microbiol*. **16**, 3128–3142 (2014).

72. Caputi, L. et al. Community-level responses to iron availability in open ocean plankton ecosystems. *Global Biogeochem. Cycles* **33**, 391–419 (2019).
73. Loescher, C. R. et al. Facets of diazotrophy in the oxygen minimum zone waters off Peru. *ISME J*. **8**, 2180–2192 (2014).
74. Fernandez, C., Farías, L. & Ulloa, O. Nitrogen fixation in denitrified marine waters. *PLoS One* **6**, e20539 (2011).
75. Jayakumar, A., Al-Rshaidat, M. M. D., Ward, B. B. & Mulholland, M. R. Diversity, distribution, and expression of diazotroph *nifH* genes in oxygen-deficient waters of the Arabian Sea. *FEMS Microbiol. Ecol*. **82**, 597–606 (2012).
76. Turk-Kubo, K. A., Karamchandani, M., Capone, D. G. & Zehr, J. P. The paradox of marine heterotrophic nitrogen fixation: abundances of heterotrophic diazotrophs do not account for nitrogen fixation rates in the Eastern Tropical South Pacific. *Environ. Microbiol*. **16**, 3095–3114 (2014).
77. Jayakumar, A. et al. Biological nitrogen fixation in the oxygen-minimum region of the eastern tropical North Pacific ocean. *ISME J.* **11**, 2356–2367 (2017).
78. Kimor, B. & Golandsky, B. Microplankton of the Gulf of Elat: Aspects of seasonal and bathymetric distribution. *Mar. Biol*. **42**, 55–67 (1977).
79. Gordon, N., Angel, D. L., Neorl, A., Kress, N. & Kimor, B. Heterotrophic dinoflagellates with symbiotic cyanobacteria and nitrogen limitation in the Gulf of Aqaba. *Mar. Ecol. Prog. Ser.* **107**, 83–88 (1994).
80. Post, A. F. et al. Spatial and temporal distribution of *Trichodesmium* spp. in the stratified Gulf of Aqaba, Red Sea. *Mar. Ecol. Prog. Ser.***239**, 241–250 (2002).
81. Foster, R. A., Paytan, A. & Zehr, J. P. Seasonality of N_2 fixation and *nifH* gene diversity in the Gulf of Aqaba (Red Sea). *Limnol. Oceanogr.* **54**, 219–233 (2009).
82. Lannes, R., Olsson-Francis, K., Lopez, P. & Bapteste, E. Carbon fixation by marine ultrasmall prokaryotes. *Genome Biol. Evol*. **11**, 1166–1177 (2019).
83. Pati, A. et al. Complete genome sequence of *Arcobacter nitrofigilis* type strain (CI). *Stand. Genomic Sci*. **2**, 300–308 (2010).
84. Belgrano, A., Allen, A. P., Enquist, B. J. & Gillooly, J. F. Allometric scaling of maximum population density: a common rule for marine phytoplankton and terrestrial plants. *Ecol. Lett*. **5**, 611–613 (2002).
85. Gaby, J. C. & Buckley, D. H. The use of degenerate primers in qPCR analysis of functional genes can cause dramatic quantification bias as revealed by investigation of *nifH* primer performance. *Microb. Ecol*. **74**, 701–708 (2017).
86. Kembel, S. W., Wu, M., Eisen, J. A. & Green, J. L. Incorporating 16S gene copy number information improves estimates of microbial diversity and abundance. *PLoS Comput. Biol*. **8**, e1002743 (2012).
87. Angly, F. E. et al. CopyRighter: a rapid tool for improving the accuracy of microbial community profiles through lineage-specific gene copy number correction. *Microbiome* **2**, 11 (2014).
88. Zehr, J. P., Mellon, M. T. & Hiorns, W. D. Phylogeny of cyanobacterial *nifH* genes: evolutionary implications and potential applications to natural assemblages. *Microbiology* **143**, 1443–1450 (1997).
89. Thiel, T. & Pratte, B. S. Regulation of three nitrogenase gene clusters in the cyanobacterium *Anabaena variabilis* ATCC 29413. *Life* **4**, 944–967 (2014).

90. Langlois, R. J., Hümmer, D. & LaRoche, J. Abundances and distributions of the dominant *nifH* phylotypes in the Northern Atlantic Ocean. *Appl. Environ. Microbiol*. **74**, 1922–1931 (2008).
91. Li, H. & Durbin, R. Fast and accurate short read alignment with Burrows-Wheeler transform. *Bioinformatics* **25**, 1754–1760 (2009).
92. Fu, L., Niu, B., Zhu, Z., Wu, S. & Li, W. CD-HIT: accelerated for clustering the next-generation sequencing data. *Bioinformatics* **28**, 3150–3152 (2012).
93. Chen, I.-M. A. et al. IMG/M v.5.0: an integrated data management and comparative analysis system for microbial genomes and microbiomes. *Nucleic Acids Res*. **47**, D666–D677 (2019).
94. Zehr, J. P. & Turner, P. J. Nitrogen fixation: Nitrogenase genes and gene expression. in *Methods in Microbiology* 271–286 (Elsevier, 2001).
95. Keeling, P. J. et al. The Marine Microbial Eukaryote Transcriptome Sequencing Project (MMETSP): illuminating the functional diversity of eukaryotic life in the oceans through transcriptome sequencing. *PLoS Biol*. **12**, e1001889 (2014).
96. Lin, Z., Kong, H., Nei, M. & Ma, H. Origins and evolution of the *recA*/*RAD51* gene family: evidence for ancient gene duplication and endosymbiotic gene transfer. *Proc. Natl. Acad. Sci. U. S. A*. **103**, 10328–10333 (2006).
97. Fujita, Y. & Bauer, C. E. Reconstitution of light-independent protochlorophyllide reductase from purified bchl and BchN-BchB subunits. In vitro confirmation of nitrogenase-like features of a bacteriochlorophyll biosynthesis enzyme. *J. Biol. Chem*. **275**, 23583–23588 (2000).
98. Katoh, K. & Toh, H. Improved accuracy of multiple ncRNA alignment by incorporating structural information into a MAFFT-based framework. *BMC Bioinformatics* **9**, 212 (2008).
99. Abascal, F., Zardoya, R. & Telford, M. J. TranslatorX: multiple alignment of nucleotide sequences guided by amino acid translations. *Nucleic Acids Res*. **38**, W7–13 (2010).
100. Guindon, S. et al. New algorithms and methods to estimate maximum-likelihood phylogenies: assessing the performance of PhyML 3.0. *Syst. Biol*. **59**, 307–321 (2010).
101. Hingamp, P. et al. Exploring nucleo-cytoplasmic large DNA viruses in *Tara* Oceans microbial metagenomes. *ISME J*. **7**, 1678–1695 (2013).
102. Props, R. et al. Absolute quantification of microbial taxon abundances. *ISME J*. **11**, 584–587 (2017).
103. Distel, D. L., Morrill, W., MacLaren-Toussaint, N., Franks, D. & Waterbury, J. *Teredinibacter turnerae* gen. nov., sp. nov., a dinitrogen-fixing, cellulolytic, endosymbiotic gamma-proteobacterium isolated from the gills of wood-boring molluscs (Bivalvia: Teredinidae). *Int. J. Syst. Evol. Microbiol*. **52**, 2261–2269 (2002).
104. Lalucat, J., Bennasar, A., Bosch, R., García-Valdés, E. & Palleroni, N. J. Biology of *Pseudomonas stutzeri*. *Microbiol. Mol. Biol. Rev*. **70**, 510–547 (2006).
105. Inomura, K., Bragg, J. & Follows, M. J. A quantitative analysis of the direct and indirect costs of nitrogen fixation: a model based on *Azotobacter vinelandii. ISME J*. **11**, 166–175 (2017).
106. Romanenko, L. A., Tanaka, N., Svetashev, V. I. & Falsen, E. Description of *Cobetia amphilecti* sp. nov., *Cobetia litoralis* sp. nov. and *Cobetia pacifica* sp. nov., classification of *Halomonas halodurans* as a later heterotypic synonym of *Cobetia*

marina and emended descriptions of the genus *Cobetia* and *Cobetia marina*. *Int. J. Syst. Evol. Microbiol*. **63**, 288–297 (2013).

107. Ramana, V. V. et al. Descriptions of *Rhodopseudomonas parapalustris* sp. nov., *Rhodopseudomonas harwoodiae* sp. nov. and *Rhodopseudomonas pseudopalustris* sp. nov., and emended description of *Rhodopseudomonas palustris*. *Int. J. Syst. Evol. Microbiol*. **62**, 1790–1798 (2012).
108. Alfaro-Espinoza, G. & Ullrich, M. S. *Marinobacterium mangrovicola* sp. nov., a marine nitrogen-fixing bacterium isolated from mangrove roots of *Rhizophora mangle*. *Int. J. Syst. Evol. Microbiol*. **64**, 3988–3993 (2014).
109. Picheral, M., Colin, S. & Irisson, J.-O. EcoTaxa, a tool for the taxonomic classification of images. http://ecotaxa.obs-vlfr.fr (2017).
110. Murphy, J. & Riley, J. P. A modified single solution method for the determination of phosphate in natural waters. *Anal. Chim. Acta* **27**, 31–36 (1962).
111. Bendschneider, K., & Robinson, R. J. A new spectrophotometric method for the determination of nitrite in sea water. *J. Mar. Res*. **11**, 87–96 (1952).
112. Aumont, O., Ethé, C., Tagliabue, A., Bopp, L. & Gehlen, M. PISCES-v2: an ocean biogeochemical model for carbon and ecosystem studies. *Geosci. Model Dev.* **8**, 2465–2513 (2015).
113. Wickham, H. *ggplot2*: Elegant graphics for data analysis. (Springer Science & Business Media, 2009).
114. Oksanen, J. et al. *vegan*: Community ecology package. https://cran.r-project.org/web/packages/vegan/index.html (2019).

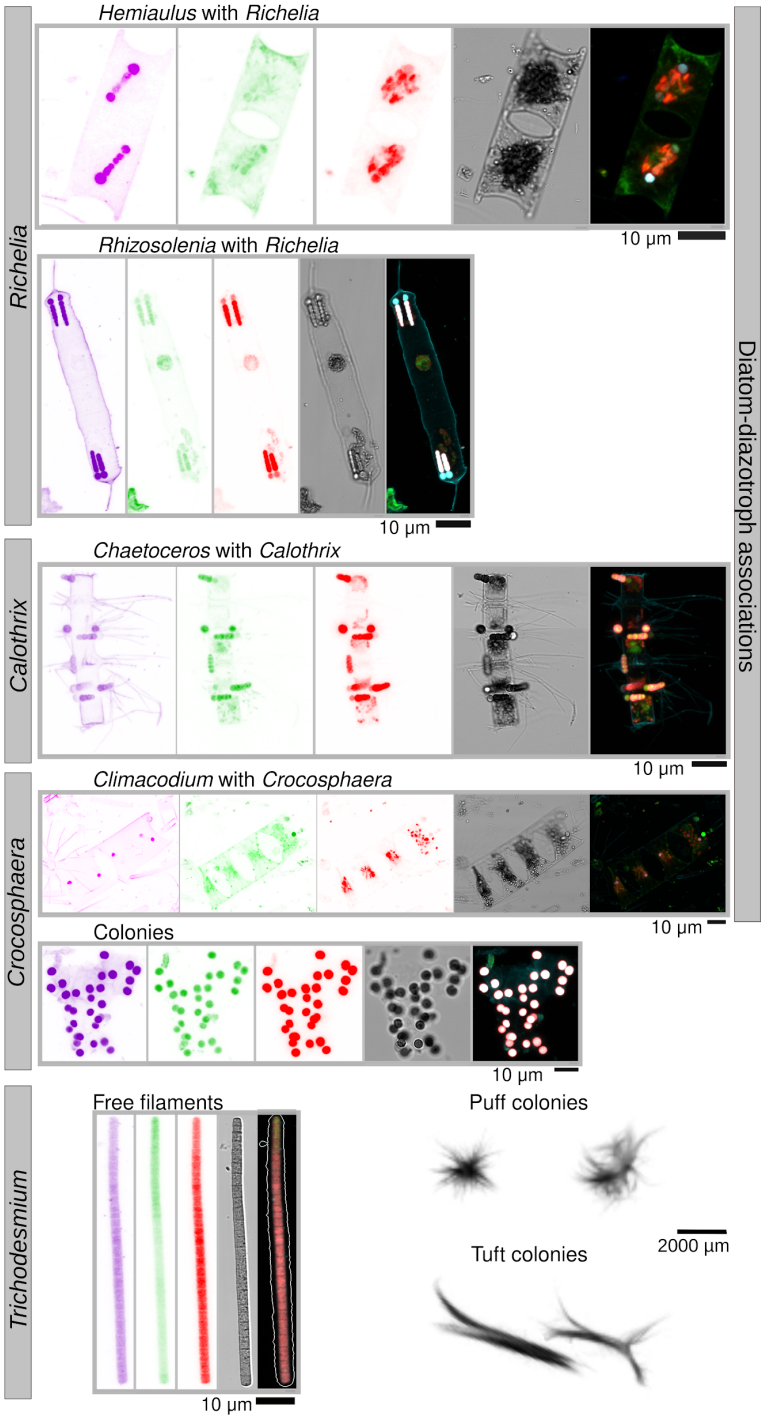

Figure 1: Imaging observations of diazotrophs in *Tara* Oceans samples. Images were obtained by environmental High Content Fluorescence Microscopy (eHCFM; Colin et al., 2017), with the exception of *Trichodesmium* colonies , which were detected in situ using an Underwater Vision Profiler 5 (UVP5; Picheral et al., 2010). From left to right, the displayed channels for each micrograph correspond to cell surface (cyan, AlexaFluor 546), cellular membranes (green, DiOC6), chlorophyll autofluorescence (red), the bright field, and the merged channels. The displayed *Hemiaulus-Richelia* association was detected at station TARA_80 in the South Atlantic Ocean, *Rhizosolenia-Richelia* at TARA_53 in the Indian Ocean, *Chaetoceros-Calothrix* at TARA_131 (ALOHA) in the North Pacific Ocean, *Climacodium-Croscophaera* at TARA_140 in the North Pacific Ocean, the *Croscophaera*-like colony at TARA_53 in the Indian Ocean, the *Trichodesmium* filament at TARA_42 in the Indian Ocean, and the *Trichodesmium* colonies at TARA_141 and TARA_142 in the North Atlantic Ocean.

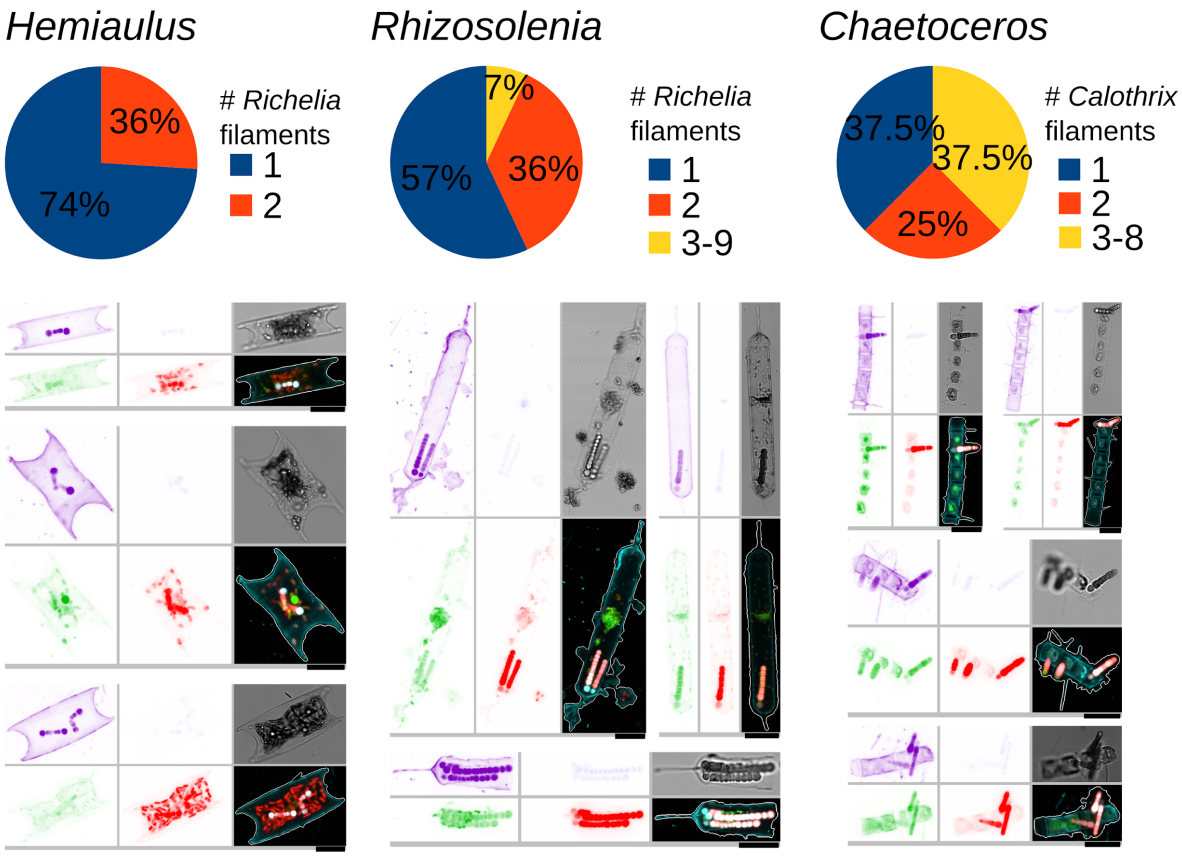

Figure 2: Variation in the number of *Richelia*/*Calothrix* filaments among the diatom-diazotroph associations observed by high-throughput confocal microscopy. Examples of images are shown. From top left to bottom right, the displayed channels for each micrograph correspond to cell surface (cyan, AlexaFluor 546 dye), DNA (blue, Hoechst dye), cellular membranes (green, DiOC6 dye), chlorophyll autofluorescence (red), the bright field, and the merged channels. The size bar at the bottom left of each microscopy image corresponds to 10 µm.

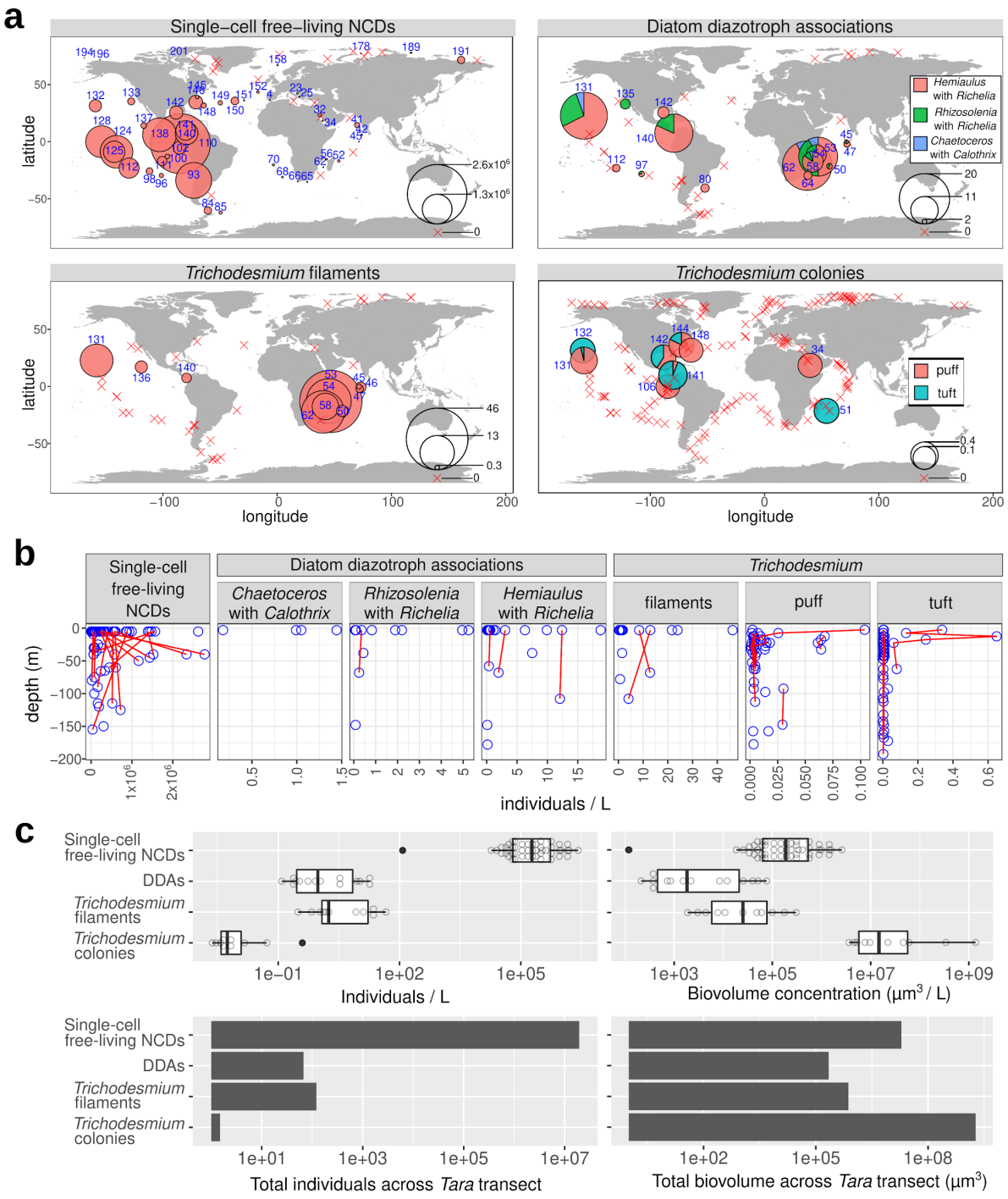

Figure 3: Abundance and distribution of diazotrophs by quantitative imaging methods. (**a**) Biogeography in surface waters. Bubble size varies according to the corresponding diazotroph concentration (individuals/L), while crosses indicate their absence. Station labels with detection of diazotrophs are indicated in blue. (**b**) Depth partition. Samples from the same geographical site are connected by lines. (**c**) Distribution of individual abundances and biomass in surface waters. Single-cell free-living non-cyanobacterial diazotrophs (NCDs) were quantified by merging flow cytometry counts with *nifH*/*recA* ratio from metagenomes from size fraction 0.22-1.6/3 µm and assuming an average cellular biovolume of 1 µm^3 based on the cell dimensions reported in the literature for cultured NCDs. The detection and biovolume determinations of diatom-diazotroph associations (DDAs) and *Trichodesmium* free filaments were carried out by high-throughput confocal microscopy in samples from the 20-180 µm size fraction. In the case of *Trichodesmium* colonies, it was determined using *in situ* images from the UVP5 .

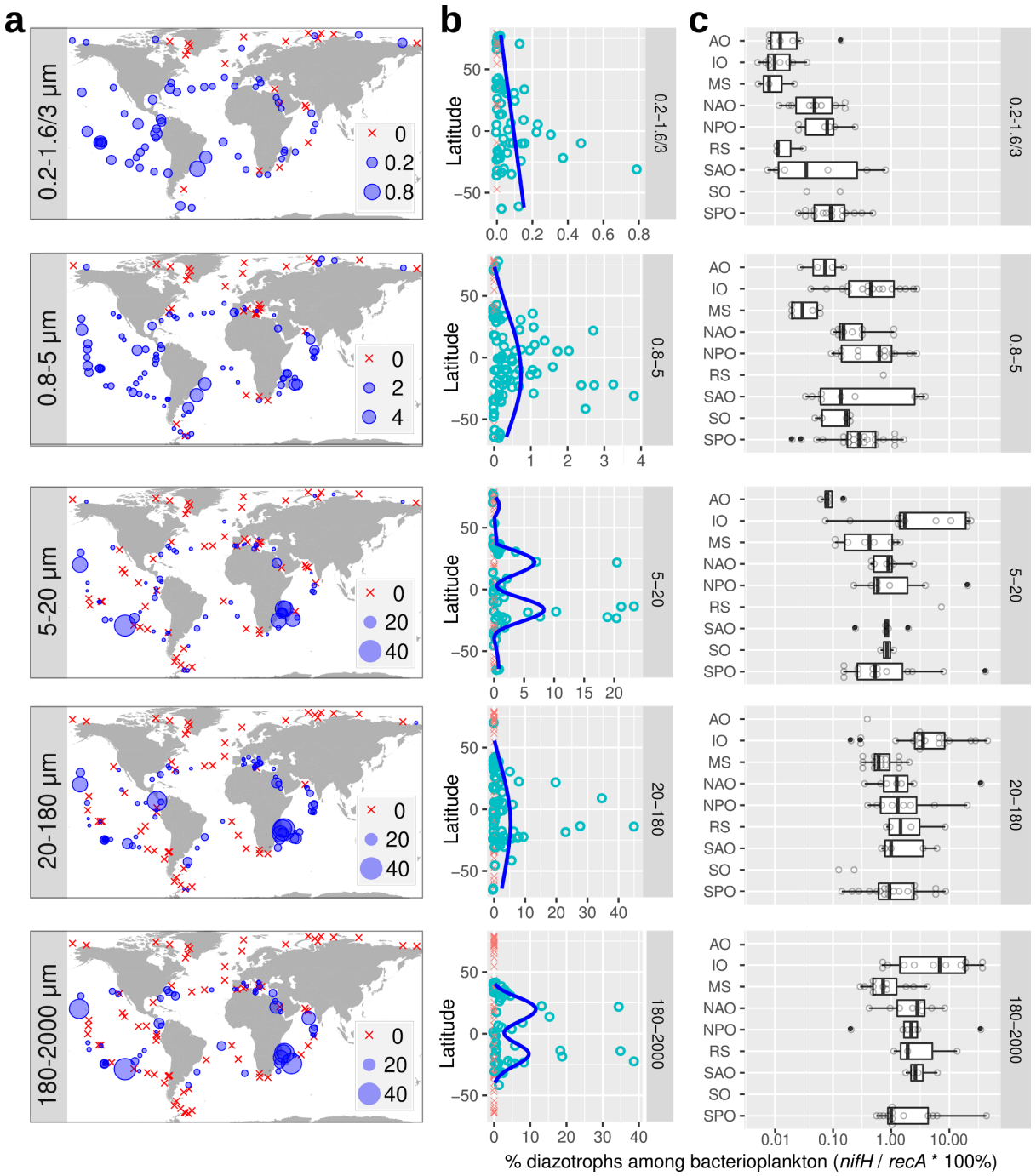

Figure 4: Biogeography of diazotrophs in surface waters using metagenomes obtained from different size-fractionated samples. The percentage of diazotrophs in the bacterioplankton community was estimated by the ratio of metagenomic read abundance between the marker genes *nifH* and *recA*. (**a**) Biogeography. The bubble size varies according to the percentage of diazotrophs, while crosses indicate absence (i.e., no detection of *nifH* reads). (**b**) Latitudinal abundance gradient. The blue lines correspond to generalized additive model smoothings. (**c**) Ocean distribution. Abbreviations: MS, Mediterranean Sea; IO, Indian Ocean; SAO, South Atlantic Ocean; SO, Southern Ocean; SPO, South Pacific Ocean; NPO, North Pacific Ocean; NAO, North Atlantic Ocean; AO, Arctic Ocean.

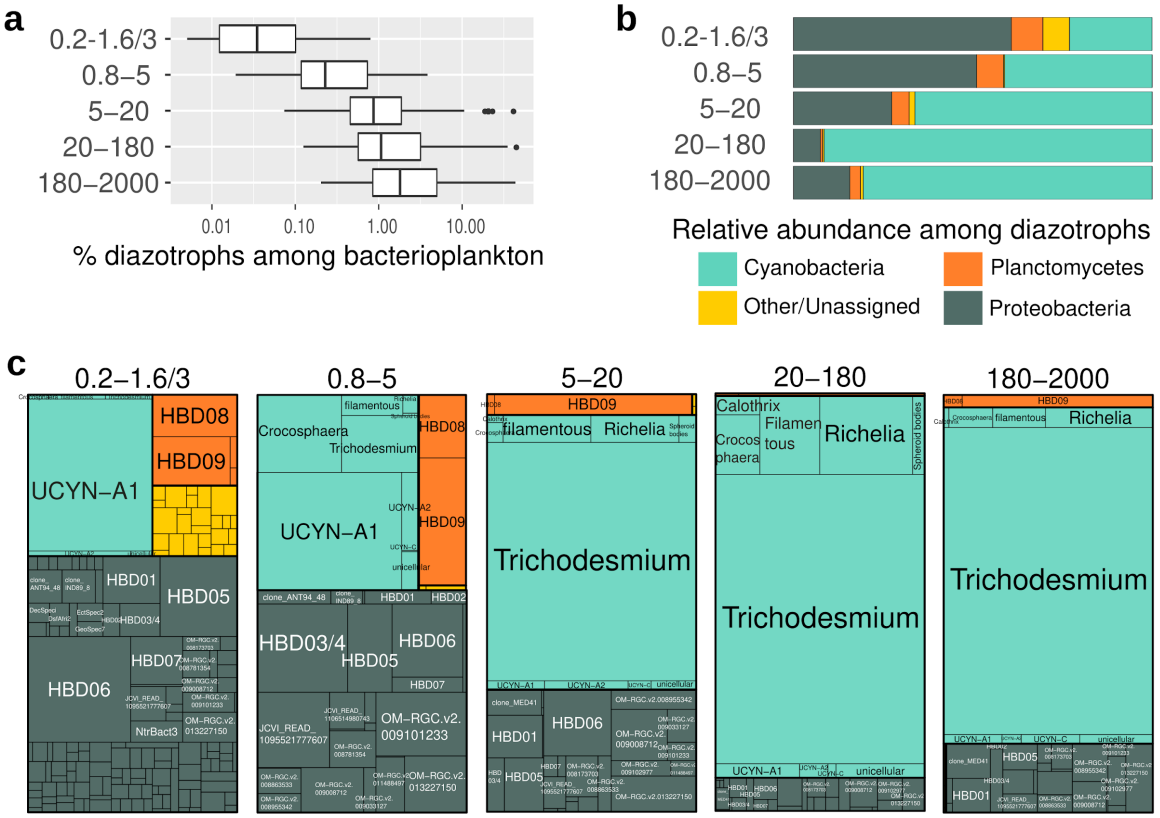

Figure 5: Abundance of diazotrophs in surface waters using metagenomes obtained from different size-fractionated samples. The percentage of diazotrophs in the bacterioplankton community was estimated by the ratio of metagenomic read abundance between the marker genes *nifH* and *recA*. (**a**) Diazotroph abundance. (**b**) Taxonomic distribution. (**c**) Taxonomic distribution at deeper resolution.

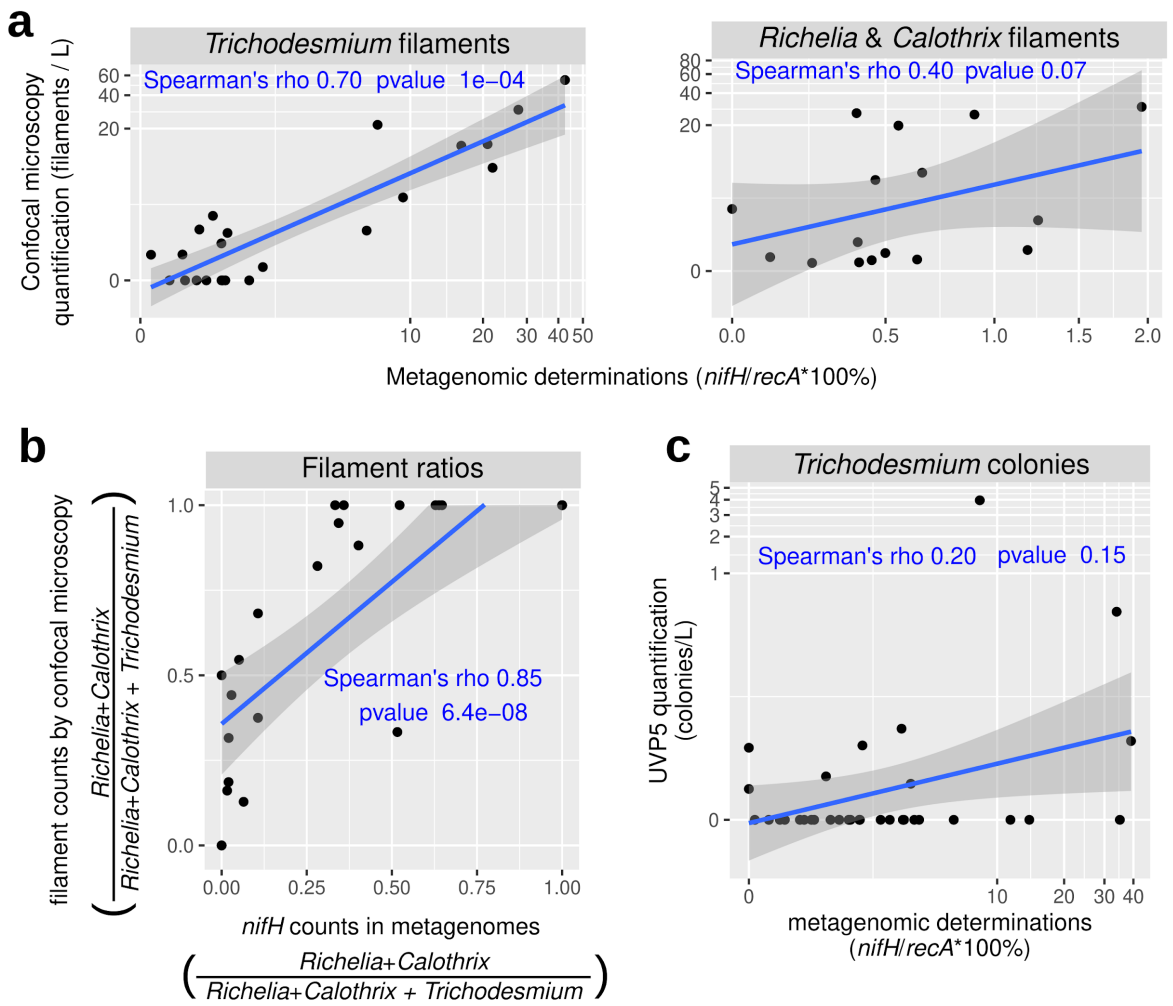

Figure 6: Correlation analysis between diazotroph quantifications by imaging and molecular methods. (**a-b**) Comparison between high-throughput confocal microscopy and metagenomics. *Calothrix*, *Richelia* and *Trichodesmium* in samples from size fraction 20-180 µm were measured by quantification of high-throughput confocal microscopy images (filaments L^{-1}) and by metagenomic counts (% of diazotrophs in the bacterioplankton community by the ratio between the marker genes *nifH* and *recA*). (**a**) Correlation of relative abundances in metagenomes and absolute abundances by confocal microscopy for the three taxa. (**b**) Correlation between the ratio of abundances between taxa. (**c**) Comparison between UVP5 and metagenomics. *Trichodesmium* colonies were measured by UVP5 quantification (colonies L^{-1}) and by metagenomic counts in the 180-2000 µm size-fractionated samples. Spearman rho correlation coefficients and p-values are displayed in blue.

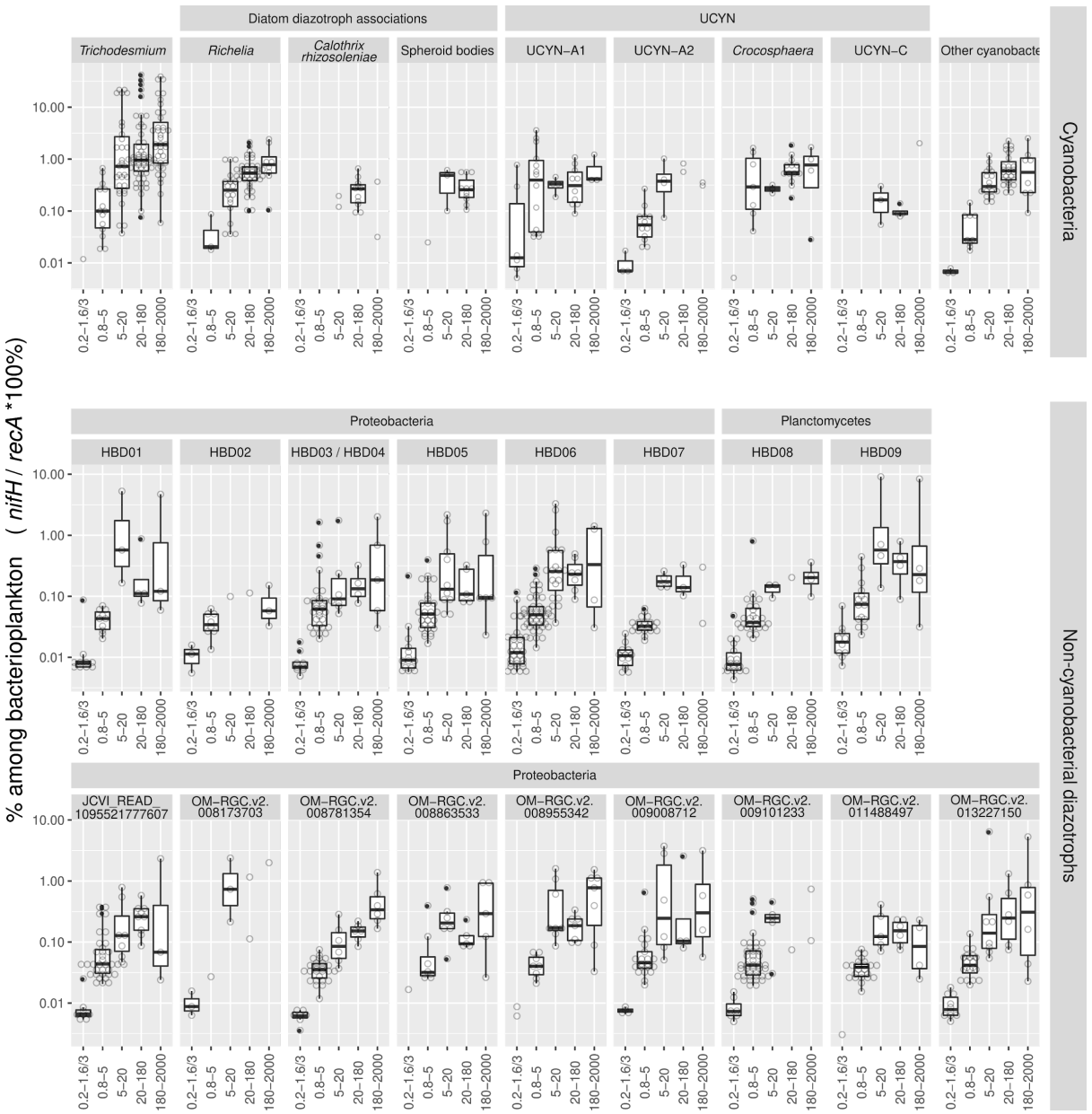

Figure 7: Distribution of the main diazotroph taxa across metagenomes obtained in different size-fractionated samples from surface waters. For each taxon, the percentage in the bacterioplankton community is estimated by the ratio of metagenomic read abundance between the marker genes *nifH* and *recA*. The lineages grouped into 'Other cyanobacteria' are displayed in Supplementary Table S1. The 'OM-RGC.v2' prefix indicates the the *nifH* sequences assembled from the metagenomes of <3 µm size fractions (Salazar al., 2019), while HBD01 to HBD09 corresponds to the metagenome-assembled genomes from the same samples (Delmont et al 2018).

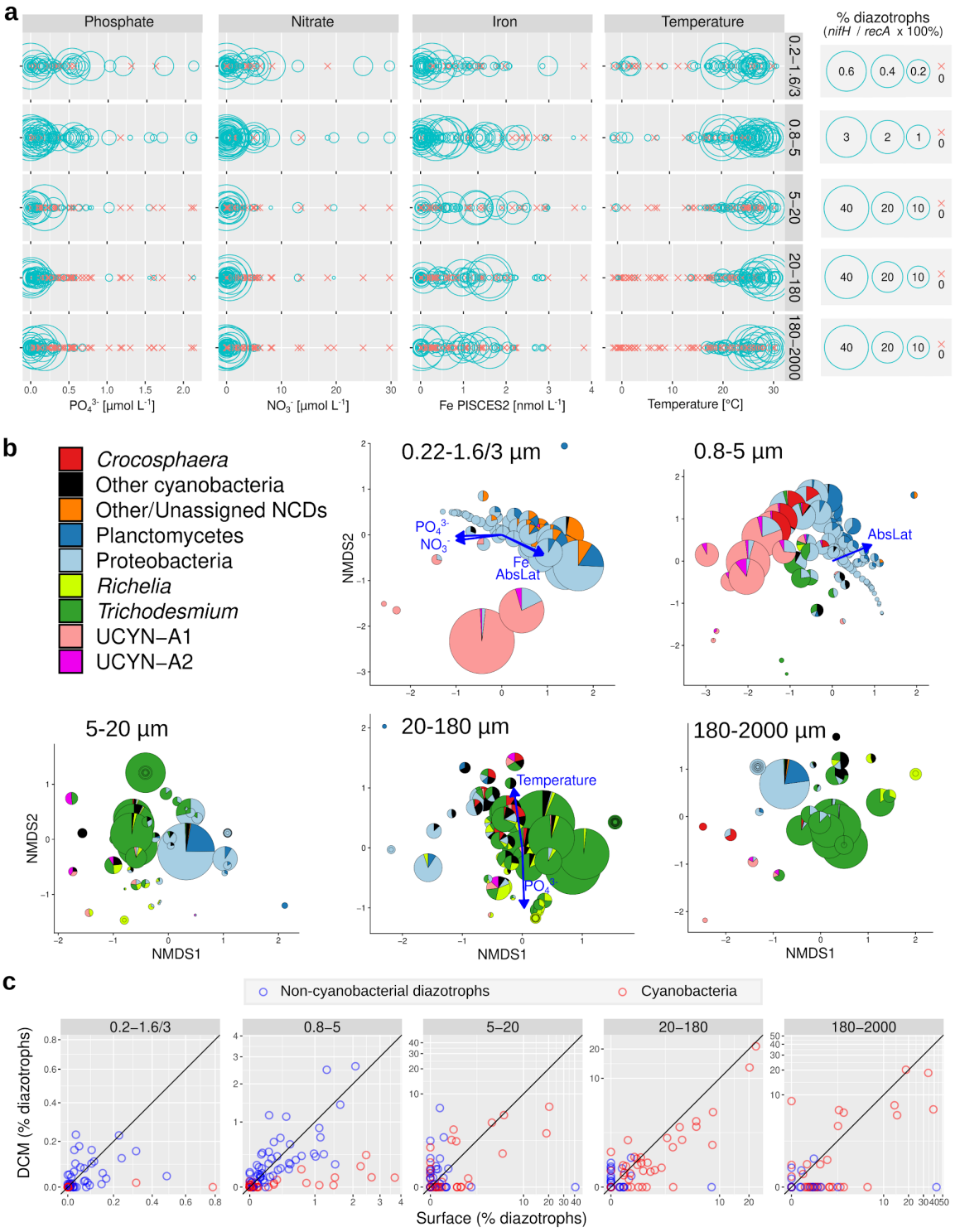

Figure 8: Environmental parameters and diazotroph distributions. (**a**) Distribution across gradients of nutrients and temperature in surface waters. Circles correspond to samples with diazotrophs, while crosses indicate absence (i.e., no detection of *nifH* reads). (**b**) NMDS analysis of stations according to Bray–Curtis distance between diazotroph communities of size-fractionated surface samples. Fitted statistically significant physico-chemical parameters are displayed (adjusted *P* value < 0.05). NMDS stress values: 0.07276045, 0.1122258, 0.1452893, 0.09693721, and 0.07969211. (**c**) Depth distribution. The scatter plots compare the diazotroph abundances between surface (5 m) and deep chlorophyll maximum (DCM; 17-180 m) for cyanobacteria (red points) and non-cyanobacterial diazotrophs (NCDs, blue points). Axes are in the same scale and the diagonal line corresponds to a 1:1 slope.

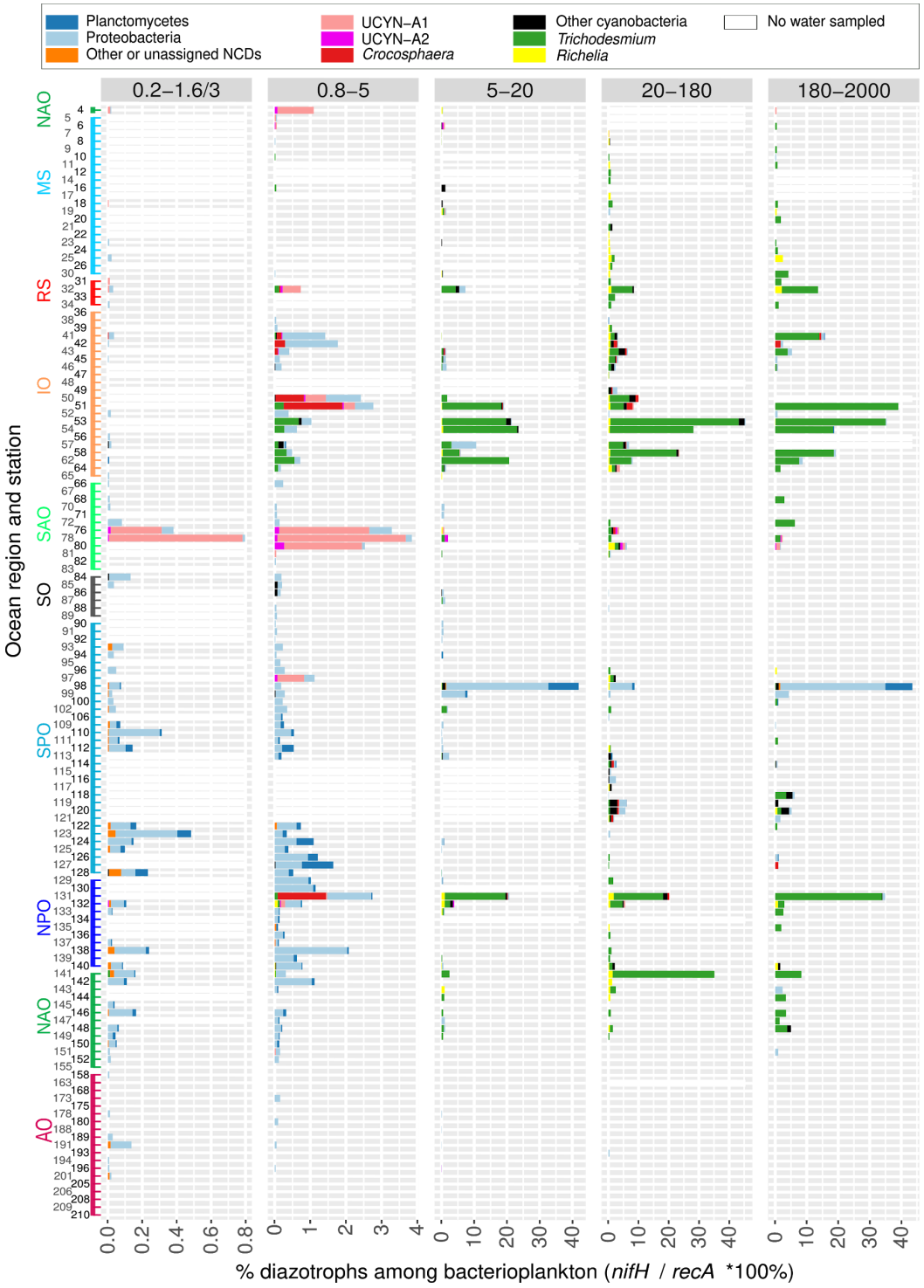

Figure 9: Diazotroph community based on metagenomes from size-fractionated surface samples. The percentage of diazotrophs in the bacterioplankton community was estimated by the ratio of metagenomic read abundance between the marker genes *nifH* and *recA*. The bar color code shows the taxonomic annotation, while the absence of water sample is indicated by a white bar. The Y axis shows the *Tara* Oceans stations and the ocean regions. Abbreviations: MS, Mediterranean Sea; IO, Indian Ocean; SAO, South Atlantic Ocean; SO, Southern Ocean; SPO, South Pacific Ocean; NPO, North Pacific Ocean; NAO, North Atlantic Ocean; AO, Arctic Ocean. The equivalent figure showing the DCM water layer is shown in Figure S2 (note the differences in scales between both figures, showing the higher relative abundance of diazotrophs in the surface layer).

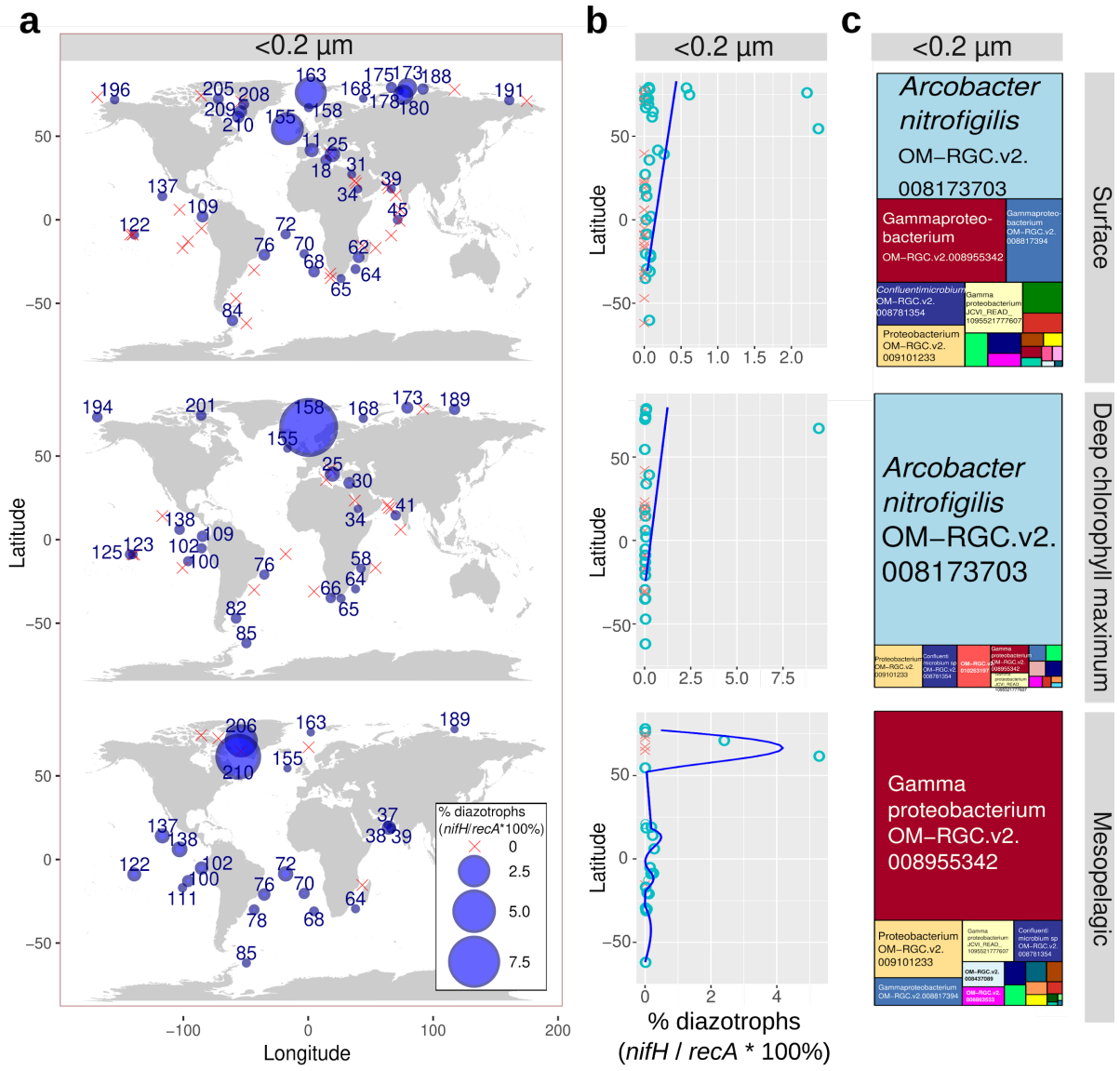

Figure 10: Detection of ultrasmall diazotrophs in metagenomes obtained from <0.22 µm size-fractionated samples of different water layers. The percentage of diazotrophs among ultrasmall bacterioplankton was estimated by the ratio of metagenomic read abundance between the marker genes *nifH* and *recA*. (**a**) Biogeography. The bubble size varies according to the percentage of diazotrophs, while crosses indicate absence (i.e., no detection of *nifH* reads). Station labels with diazotrophs detection are indicated in blue. (**b**) Latitudinal abundance gradient. Circles correspond to samples with diazotrophs, while crosses indicate absence. The blue lines correspond to generalized additive model smoothings. (**c**) Taxonomic distribution. The 'OM-RGC.v2' prefix indicates the *nifH* sequences assembled from metagenomes of <3 µm size fractions (Salazar al., 2019), including <0.22 µm.

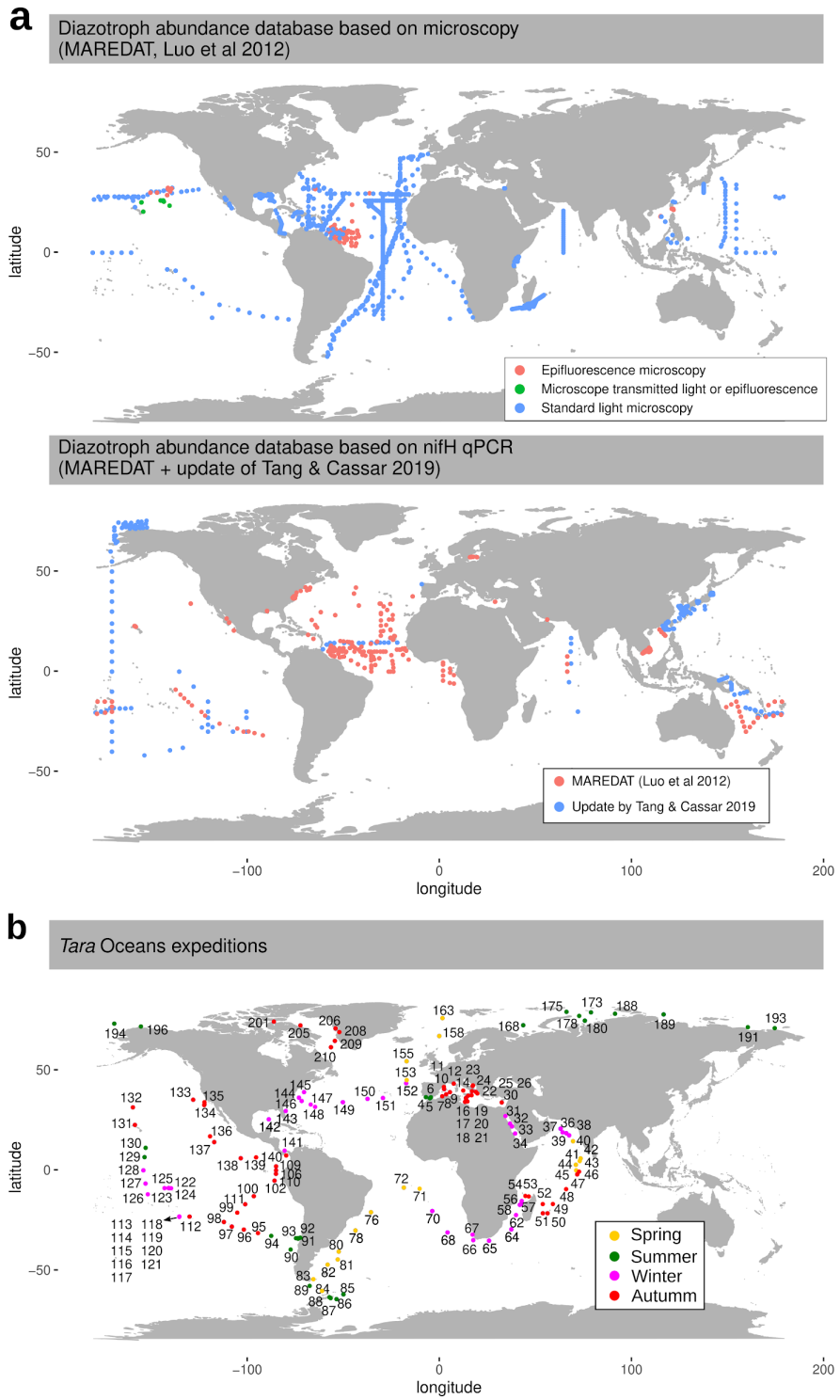

Supplementary Figure S1: Comparison between the databases of diazotroph distribution and the *Tara* Oceans expeditions. (**a**) The MARine Ecosystem DATa (MAREDAT) includes a database for microscopy counts (upper map) and for quantitative PCR targeting the *nifH* gene (lower map). The microscopy only covers *Trichodesmium* and diatom-diazotroph associations and it is a compilation of 44 different publications between 1966 and 2011 (Luo et al., 2012). The *nifH* dataset includes *Trichodesmium*, diatom-diazotroph associations, UCYN-A, *Crocosphaera* (UCYN-B) and UCYN-C and it is the result of 19 publications between 2005 and 2011 (red points; Luo et al., 2012). This later dataset has been recently updated by Tang and Cassar (2019) with measurements from 17 new publications between 2012 and 2018 (blue points). (**b**) Sampling route of the *Tara* Oceans expeditions (2009-2013), showing station labels and sampling season.

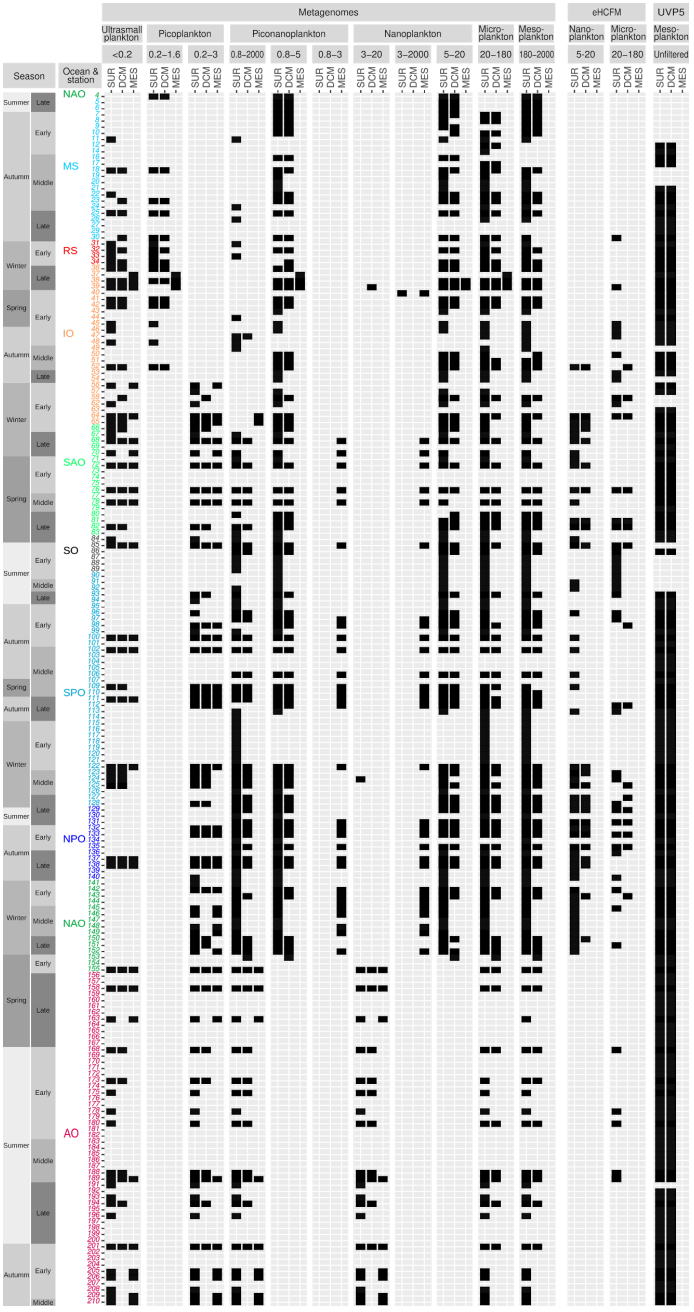

Supplementary Figure S2: Samples and methods used in this study. The current analysis of global diversity and abundance of diazotrophs was carried out across 197 *Tara* Oceans stations where samples where taken for metagenomic sequencing and/or for environmental High Content Fluorescence Microscopy (eHCFM) and/or images were taken *in situ* using an Underwater Vision Profiler 5 (UVP5). The analyzed samples are indicated as filled boxes. A complete sampling station consisted of collecting plankton from three distinct depth layers: surface (SUR), deep chlorophyll maximum (DCM), and mesopelagic (MES). The data from the bottom of the mixed layer was collected when no deep chlorophyll maximum was observed (stations TARA_123, TARA_124, TARA_125, TARA_152 and TARA_153). Plankton communities from SUR and DCM were fractionated into six main size classes: ultrasmall plankton (<0.22 µm), picoplankton (0.2 to 1.6 µm or 0.2 to 3 µm), piconanoplankton (0.8 to 5 µm or 0.8 to 2000 µm), nanoplankton (5 to 20 µm or 3 to 20 µm), microplankton (20 to 180 µm), and mesoplankton (180 to 2000 µm). For MES samples, size fractions were more heterogeneous (<0.22 µm, 0.2 to 1.6 µm, 0.2 to 3 µm, 0.8 to 3 µm, 0.8 to 5 µm, 0.8 to 200 µm, 0.8 to 2000 µm, 3-20 µm, 3-2000 µm, 5-20 µm). Season and moment of the season (early, middle, late) are displayed to the left of the panel. Station labels are coloured according to the ocean region: IO, Indian Ocean; MS, Mediterranean Sea; NAO, North Atlantic Ocean; RS, Red Sea; SAO, South Atlantic Ocean; SO, Southern Ocean; SPO, South Pacific Ocean.

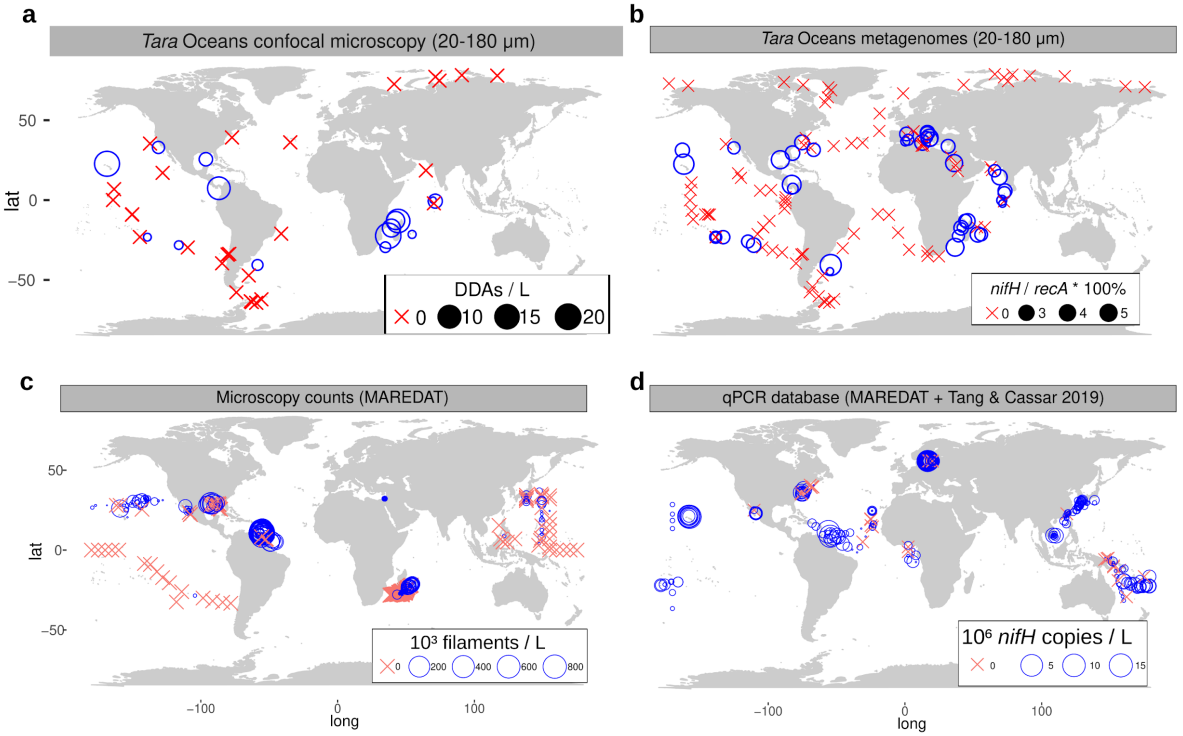

Supplementary Figure S3: Biogeography of diatom-diazotroph associations (DDAs) in surface waters. (**a-b**) Abundance across the *Tara* Oceans transect based on quantification of high-throughput confocal microscopy determinations (a) and from metagenomic read abundance of *nifH* gene (b). (**c-d**) Abundance in the MARine Ecosystem DATa (MAREDAT) database for microscopy counts (c) and for quantitative PCR targeting the *nifH* gene (d). This latter includes the recent compilation update by Tang and Cassar 2019. Bubble size varies according to the corresponding concentration, while crosses indicate their absence.

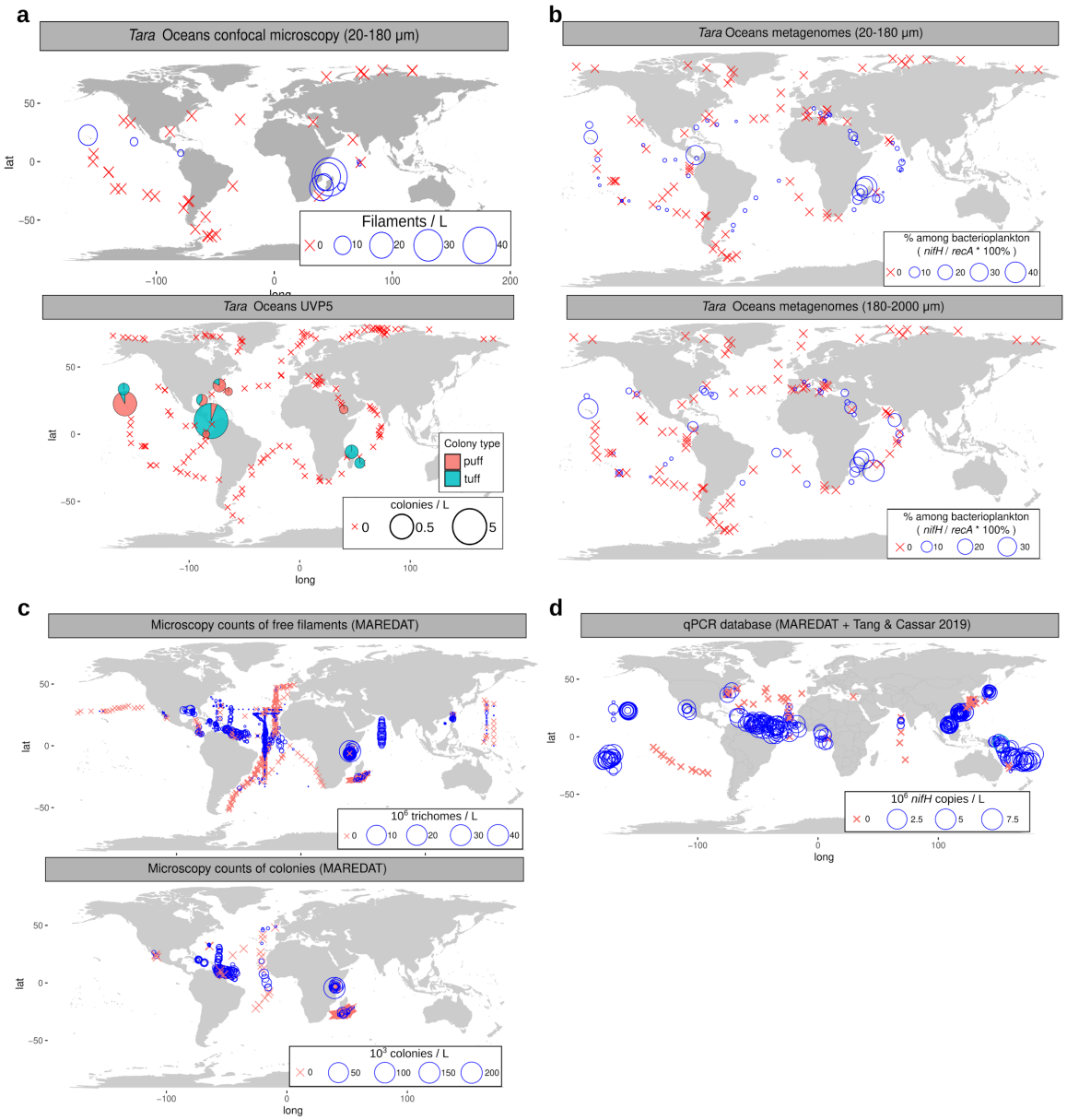

Supplementary Figure S4: Biogeography of *Trichodesmium* aggregates in surface waters. (**a**) Abundance across the *Tara* Oceans transect of free-filaments by high-throughput confocal microscopy in 20-180-µm size-fractionated samples (upper map) and colonies by Underwater Vision Profiler 5 (lower map). (**b**) Abundance across the *Tara* Oceans transect based on the metagenomic read abundance of the *nifH* marked gene in 20-180-µm and 180-2000-µm size-fractionated samples. (**c-d**) Abundance in the MARine Ecosystem DATa (MAREDAT) database for microscopy counts of free-filaments (c; upper map) and colonies (c; lower map) and for quantitative PCR targeting the *nifH* gene (d). This latter includes the recent compilation update by Tang and Cassar 2019. Bubble size varies according to the corresponding concentration, while crosses indicate their absence.

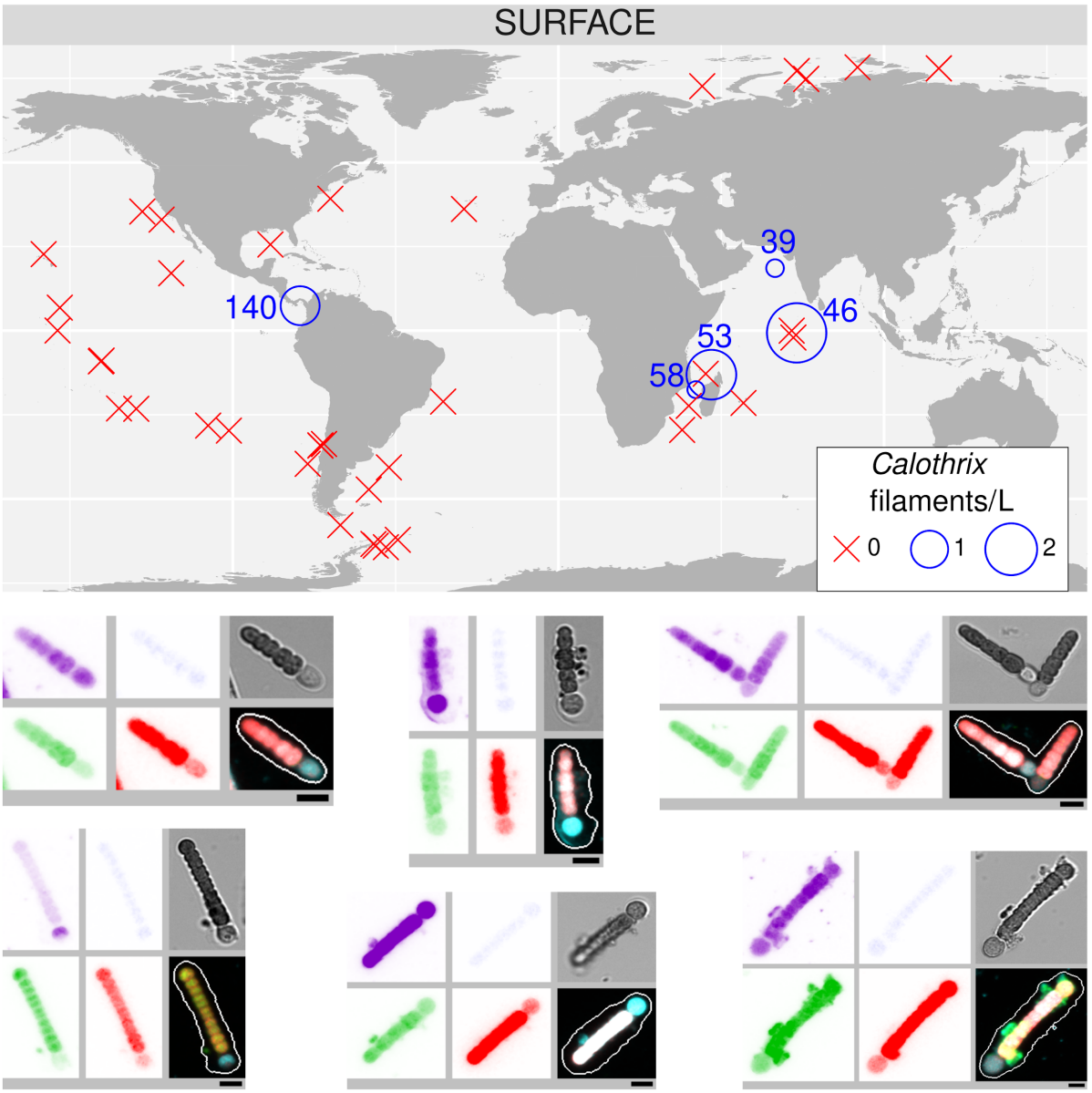

Supplementary Figure S5: Abundance and distribution of free filaments of *Richelia*/*Calothrix* in surface waters by quantification of high-throughput confocal microscopy images in samples from size fraction 20-180 µm. Maps show the biogeographical distribution. Bubble size varies according to the corresponding filament concentration, while red crosses indicate their absence. Examples of images are shown. From up left to bottom right, the displayed channels for each micrograph correspond to cell surface (cyan, AlexaFluor 546 dye), DNA (blue, Hoechst dye), cellular membranes (green, DiOC6 dye), chlorophyll autofluorescence (red), the bright field, and the merged channels. The size bar at the bottom left of each microscopy image corresponds to 2.5 µm.

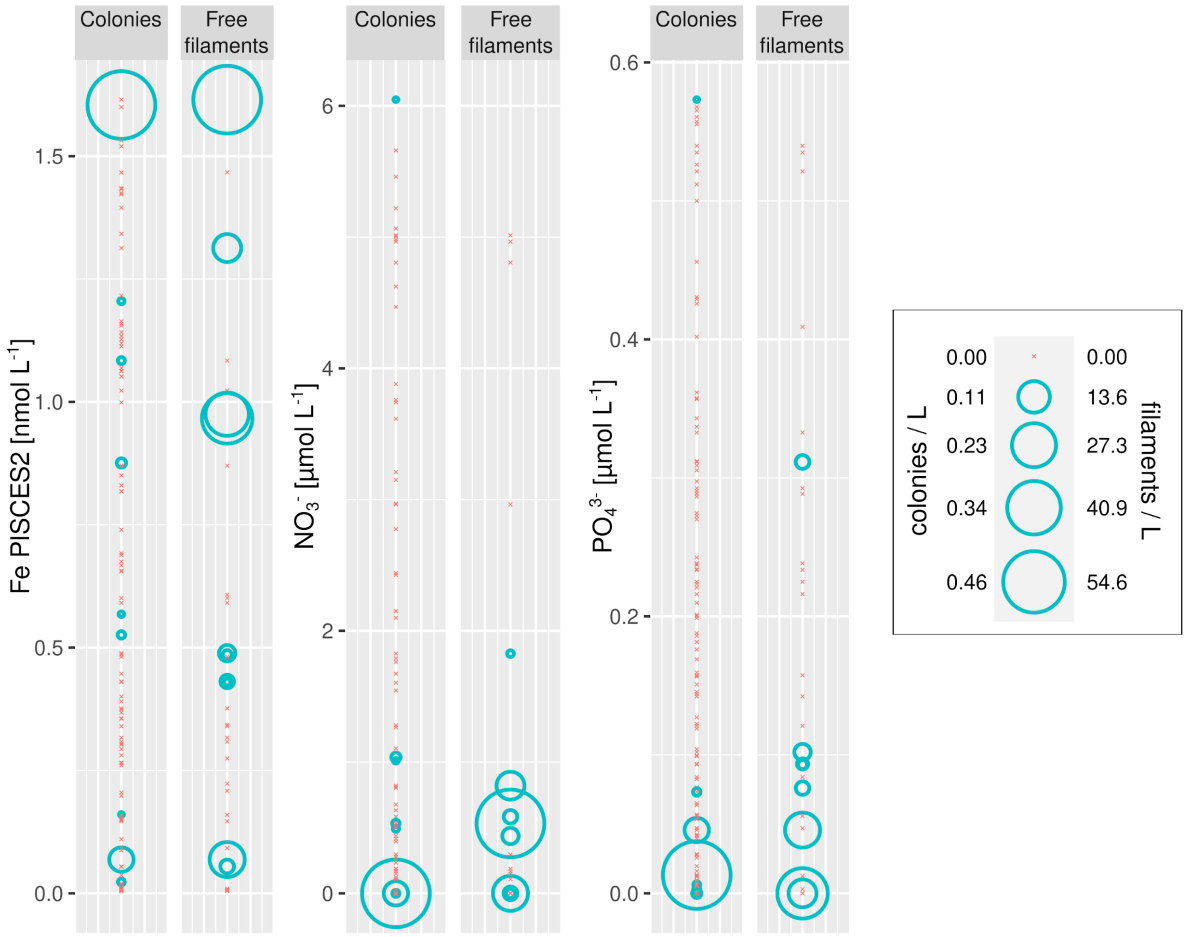

Supplementary Figure S6: *Trichodesmium* aggregation under different nutrient conditions. Bubble size varies according to the corresponding abundance of free filaments or colonies, while crosses indicate their absence. Free filaments were quantified by high-throughput confocal microscopy in samples from the 20-180 µm size fraction, while colonies were quantified using *in situ* images from the Underwater Vision Profiler 5 (UVP5).

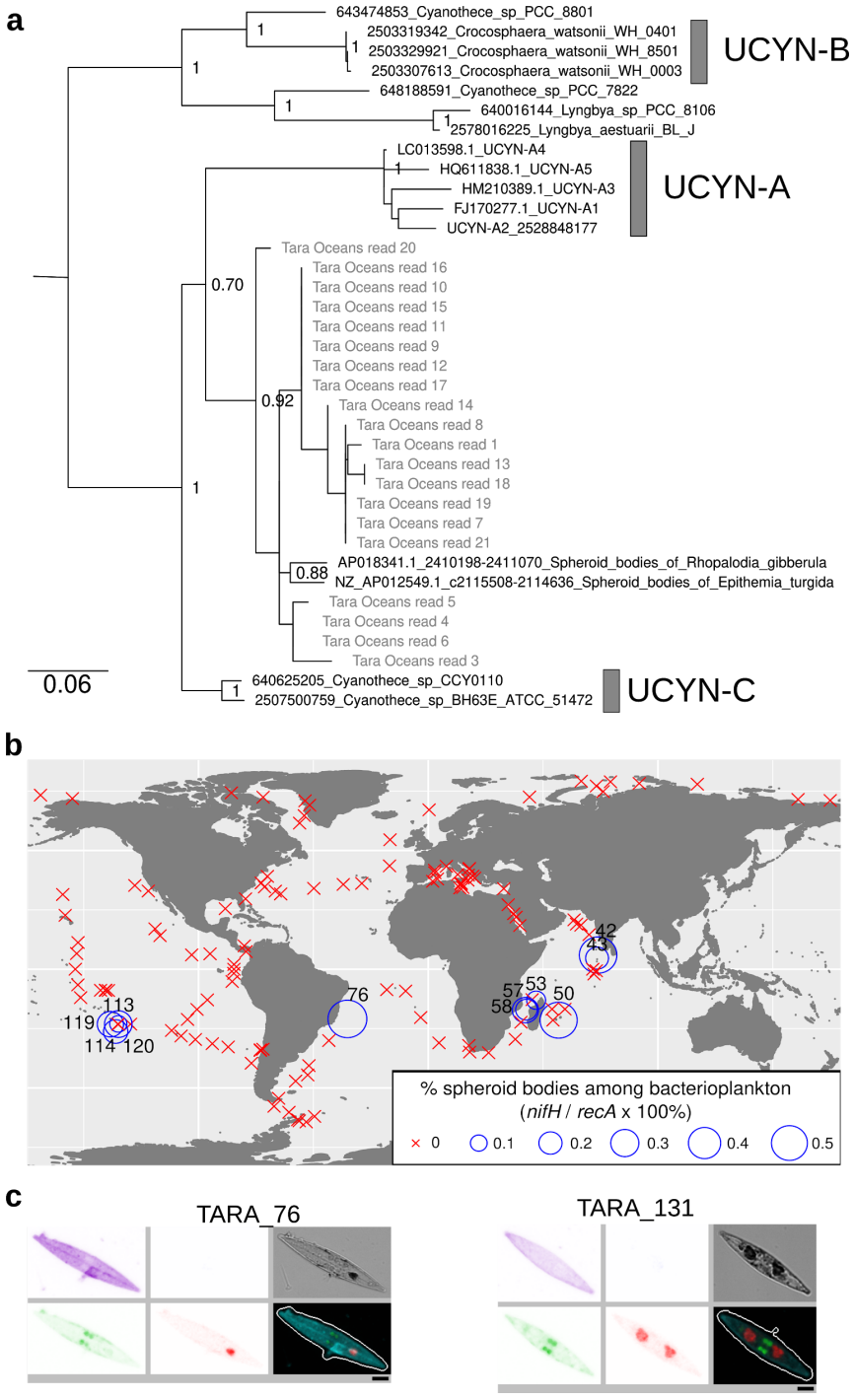

Supplementary Figure S7: Putative spheroid bodies in *Tara* Oceans samples. (**a**) Phylogeny of metagenomic reads with sequence similarity to the *nifH* gene from spheroid bodies. NCBI or IMG accession numbers of reference nucleotide sequences and the species names are indicated in the tip labels. The aLRT values are shown for the main clades. (**b**) Biogeography in surface waters of 20-180 µm size fractionated samples. The bubble size varies according to the percentage of reads of potential spheroid bodies, while crosses indicate absence (i.e., no detection of *nifH* reads). Station labels with read detection are indicated. (**c**) Images of pennate diatoms containing round granules that lack chlorophyll autofluorescence that were observed in the same samples where putative metagenomic sequences from spheroid-bodies were detected. From up left to bottom right, the displayed channels for each micrograph correspond to cell surface (cyan, AlexaFluor 546 dye), DNA (blue, Hoechst dye), cellular membranes (green, DiOC6 dye), chlorophyll autofluorescence (red), the bright field, and the merged channels. The size bar at the bottom left of each microscopy image corresponds to 2.5 µm.

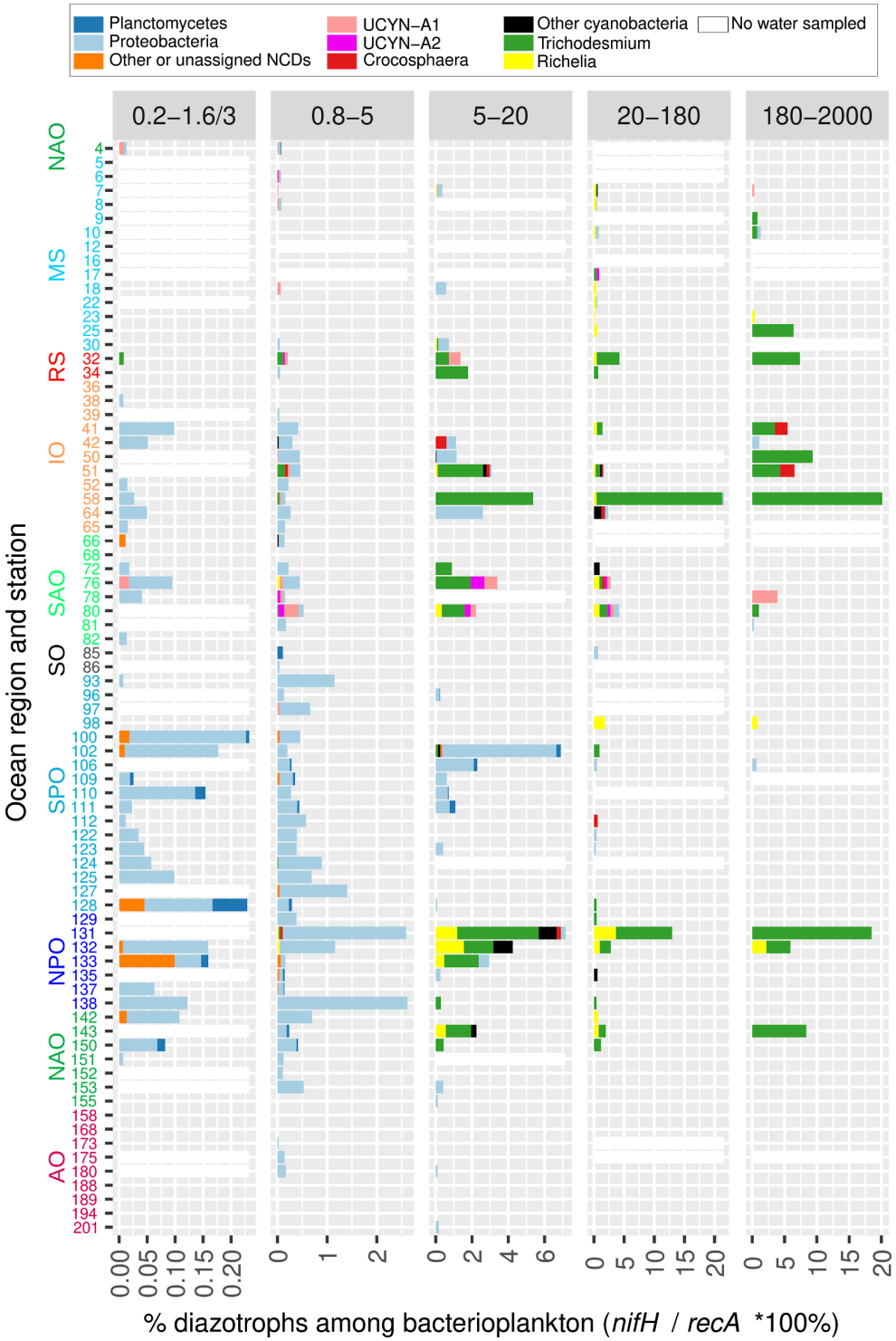

Supplementary Figure S8: Diazotroph community based on metagenomes from size-fractionated samples derived from deep-chlorophyll maxima. The percentage of diazotrophs in the bacterioplankton community was estimated by the ratio of metagenomic read abundance between the marker genes *nifH* and *recA*. The bar color code shows the taxonomic annotation, and the absence of water sample is indicated by a white bar. The Y axis shows the *Tara* Oceans stations and the ocean regions. Abbreviations: MS, Mediterranean Sea; IO, Indian Ocean; SAO, South Atlantic Ocean; SO, Southern Ocean; SPO, South Pacific Ocean; NPO, North Pacific Ocean; NAO, North Atlantic Ocean; AO, Arctic Ocean. The equivalent figure showing the surface layer is shown in Figure 7 (note the differences in scales between both figures, showing the higher relative abundance of diazotrophs in the surface layer). The data from the bottom of the mixed layer is displayed when no deep chlorophyll maximum was observed (stations TARA_123, TARA_124, TARA_125, TARA_152 and TARA_153).

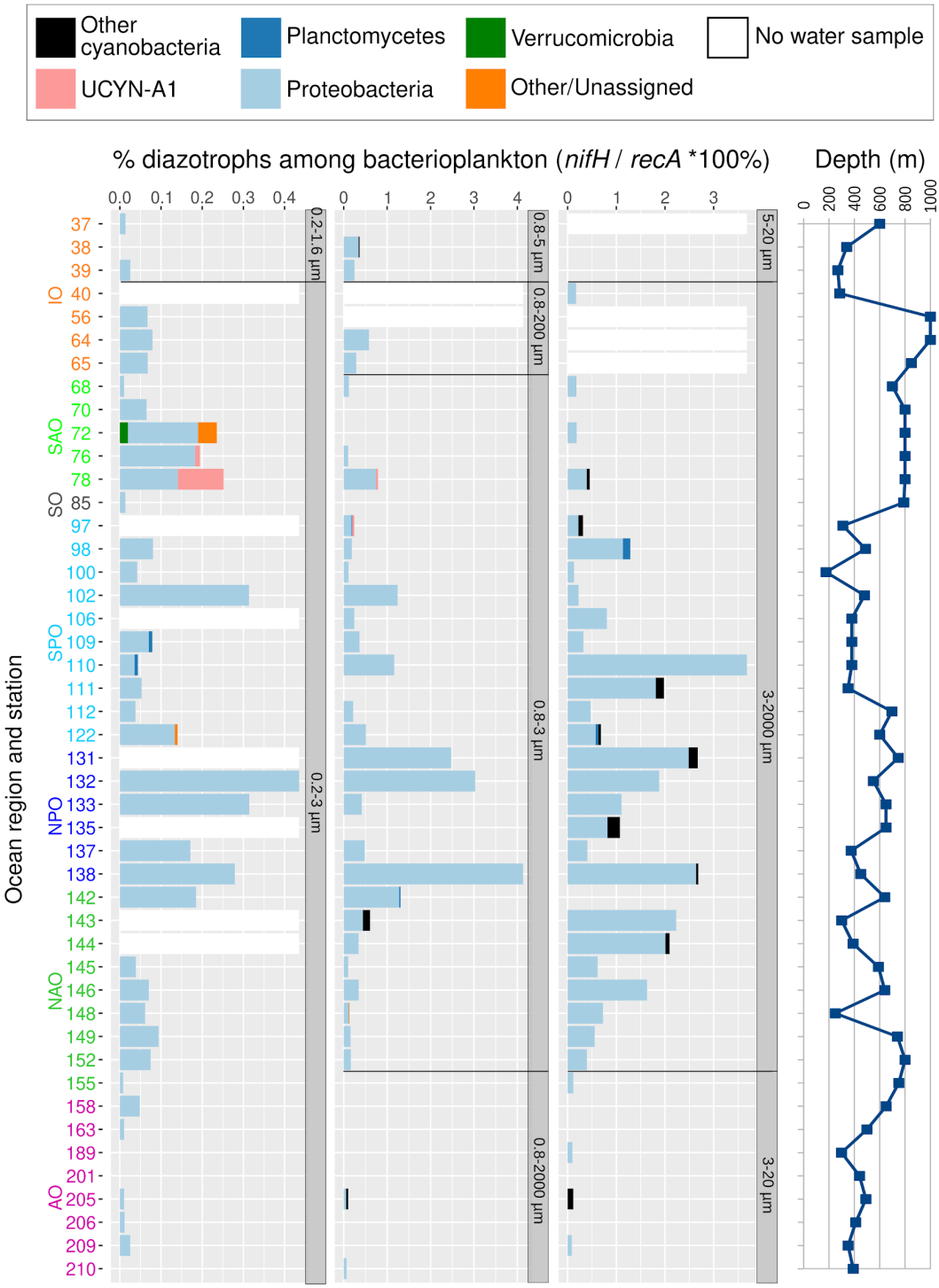

Supplementary Figure S9: Diazotroph community based on metagenomes from size-fractionated samples from mesopelagic depths. The percentage of diazotrophs in the bacterioplankton community was estimated by the ratio of metagenomic read abundance between the marker genes *nifH* and *recA*. The bar color code shows the taxonomic annotation, and the absence of water sample is indicated by a white bar. Size fractions are also indicated (they are more heterogeneous than those from surface and deep chlorophyll maximum samples). The Y axis shows the *Tara* Oceans stations and the ocean regions. Abbreviations: MS, Mediterranean Sea; IO, Indian Ocean; SAO, South Atlantic Ocean; SO, Southern Ocean; SPO, South Pacific Ocean; NPO, North Pacific Ocean; NAO, North Atlantic Ocean; AO, Arctic Ocean. Sampling depth is indicated in the right panel.

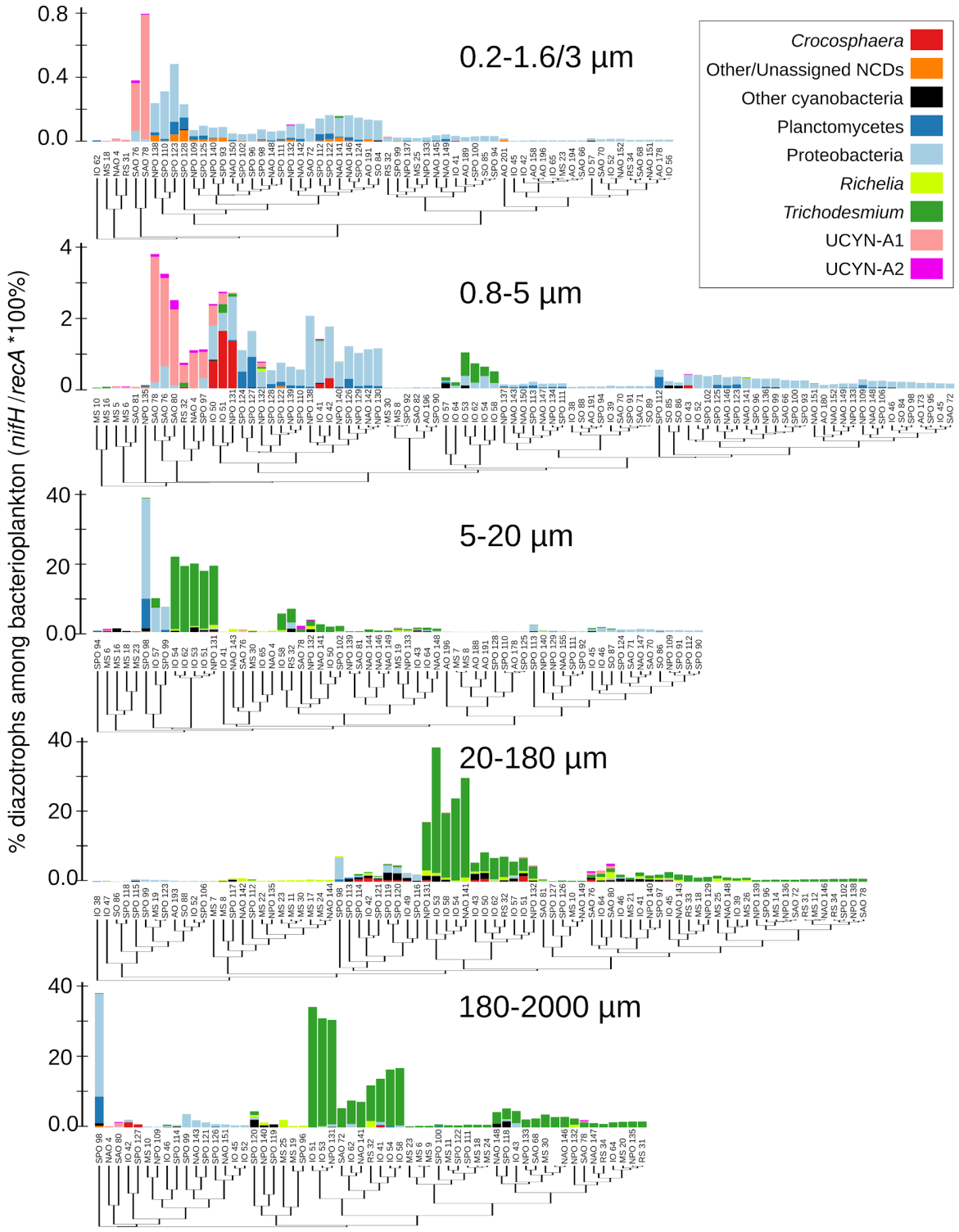

Supplementary Figure S10: Clusters of diazotroph communities based on metagenomes from size-fractionated surface samples. For each size fraction, the samples are sorted by similarity using hierarchical clustering (Bray–Curtis distance) and the corresponding diazotroph relative abundances are displayed as bar plots, with the color code according to the taxonomic annotation. The percentage of diazotrophs in the bacterioplankton community was estimated by the ratio of metagenomic read abundance between the marker genes *nifH* and *recA*. The dendrogram tip labels show the *Tara* Oceans stations and the ocean regions. Abbreviations: MS, Mediterranean Sea; IO, Indian Ocean; SAO, South Atlantic Ocean; SO, Southern Ocean; SPO, South Pacific Ocean; NPO, North Pacific Ocean; NAO, North Atlantic Ocean; AO, Arctic Ocean.

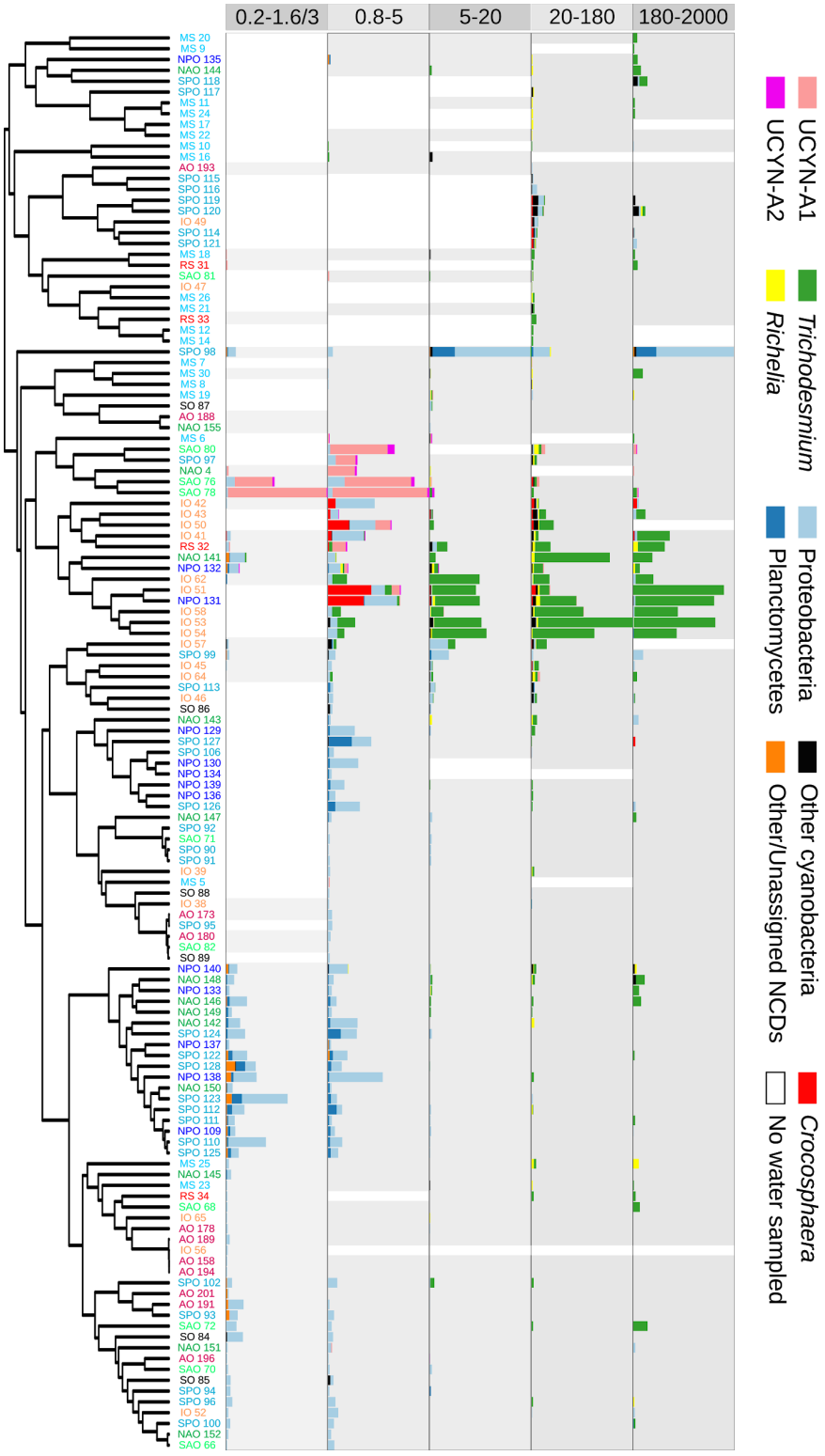

Supplementary Figure S11: Clusters of diazotroph communities based on metagenomes from size-fractionated surface samples. For each size fraction, the samples are sorted by similarity using hierarchical clustering (Bray–Curtis distance) and the corresponding diazotroph relative abundances are displayed as bar plots, with the color code according to the taxonomic annotation. The percentage of diazotrophs in the bacterioplankton community was estimated by the ratio of metagenomic read abundance between the marker genes *nifH* and *recA*. The dendrogram tip labels show the *Tara* Oceans stations and the ocean regions. Abbreviations: MS, Mediterranean Sea; IO, Indian Ocean; SAO, South Atlantic Ocean; SO, Southern Ocean; SPO, South Pacific Ocean; NPO, North Pacific Ocean; NAO, North Atlantic Ocean; AO, Arctic Ocean.

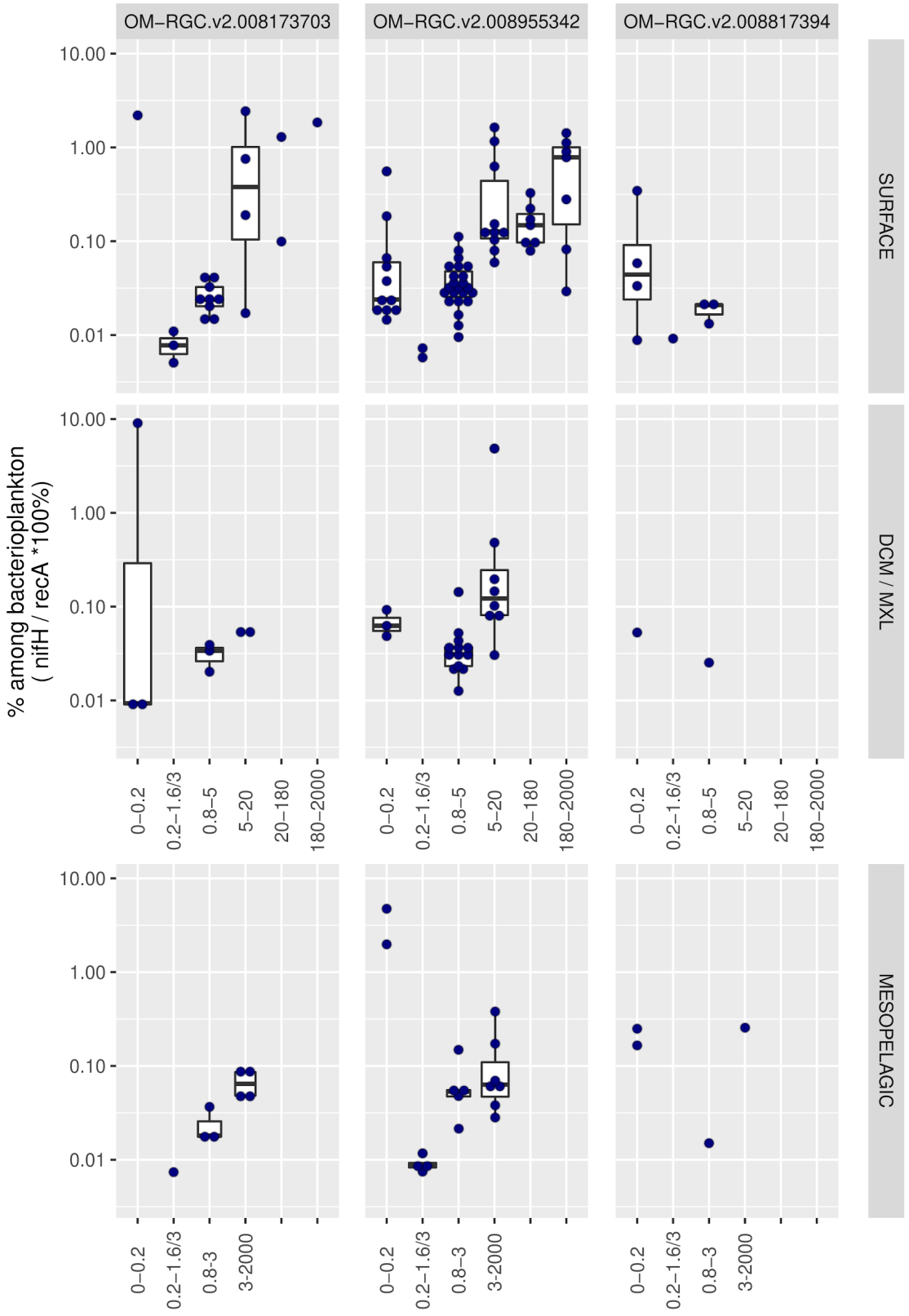

Supplementary Figure S12: Distribution of potential ultrasmall diazotrophs across metagenomes obtained in different size-fractionated samples. For each taxon, the percentage in the bacterioplankton community is estimated by the ratio of metagenomic read abundance between the marker genes *nifH* and *recA*. The 'OM-RGC.v2' prefix indicates the *nifH* sequences assembled from the metagenomes of <0.22 µm size fraction (Salazar al., 2019).